Korean J. Chem. Eng., 39(4), 853-864 (2022)
DOI: 10.1007/s11814-021-0983-1

pISSN: 0256-1115
eISSN: 1975-7220

Fuel filling time estimation for hydrogen-powered fuel cell electric vehicle at different initial conditions using dynamic simulation

Russel J. Galanido*, Leah Jessica Sebastian*, Daniel Owusu Asante*, Dong Sun Kim*, Nam-Ju Chun, and Jungho Cho*,†**

*Chemical Process Research Laboratory, Department of Chemical Engineering, Kongju National University, 275 Budae-dong, Cheonan-si, Seobuk-gu, Chungcheongnam-do 31080, Korea
**NK CO., LTD, 194-11, Gwahaksandan-ro, Gangseo-gu, Busan 46743, Korea
(*Received 12 July 2021 • Revised 10 October 2021 • Accepted 13 October 2021*)

Abstract−The hydrogen fuel filling time for hydrogen-powered fuel cell electric vehicles at different initial conditions was estimated through dynamic simulation by using Aspen Dynamics v.11 with Peng-Robinson as the thermodynamic model. The simulation process was divided into three parts, in which the different storage vessels (LP, MP, and HP banks) act as the sole hydrogen source. The SAE J2601 standard was used as the basis for the fueling operation. For the fast filling of the car tank with hydrogen gas, a detailed heat transfer modeling suited for the process was elaborated to correctly predict the in-cylinder temperature throughout the fueling operation. During the dynamic simulation, the station pressure, the state-of-charge %, the car tank temperature, the hydrogen flow rate, the amount of hydrogen gas accumulated in the car tank, and the high-pressure storage vessels' conditions were monitored and confirmed according to their expected values or limits. It is determined that the fueling times calculated in the dynamic study were faster than their corresponding estimated values for all cases, indicating the integrity of the process.

Keywords: Hydrogen Gas, Fueling Time Estimation, Storage Tanks, Fuel Cell Electric Vehicle Dynamic Simulation

INTRODUCTION

Hydrogen, an odorless, colorless, tasteless, and nonpoisonous gas, is one of the most abundant elements in the universe. It is a renewable resource found in all growing things [1]. Owing to its excellent advantages, such as comprehensive source, eco-friendly, high combustion efficiency, and reproducibility, hydrogen has become the most promising alternative fuel of the 21st century [1-4]. Most experts suggest that hydrogen as secondary energy has the elements to address all three of these concerns. In its purest form, there are zero emissions, the supply is endless, and production may use a variety of energy sources, including renewable [5-7]. However, due to its low density, hydrogen creates significant storage challenges [3,8].

Currently, hydrogen can be stored using various methods, such as compressed gas, cryogenic liquid, and metal hydride [9-15]. Among the mentioned methods, the compressed gas storage method (by high-pressure tanks) is widely used in the transportation field due to its practicality, high reliability, durability, acceptable efficiency, and affordability [8,9,16]. Two main types of tanks are currently used for hydrogen storage and compression [16]. Type III and IV tanks are both comprised of a carbon-fiber/epoxy composite external wrap. The only difference between the two tanks is the internal liner having aluminum with the former while plastic for the latter [8,17]. These types of tanks are commonly used for electric vehicles which utilize hydrogen as their fuel.

Hydrogen fuel cell electric vehicles (HFCEVs) are more economical than conventional internal combustion engine vehicles (ICEVs). It can bring drivers a comparable experience to conventional ICEVs concerning fueling time and performance, such as power and driving range, among others [18]. The advantages of HFCEVs include producing no tailpipe emissions (only water vapor), faster fueling, noiseless drive (no engine knocking), better fuel economy and efficiency, and easy maintenance [19]. However, effectively utilizing HFCEVs requires a safe and optimized method to store a sufficient amount of hydrogen.

In proving a safe delivery of hydrogen gas into the vehicle, the Society of Automotive Engineers (SAE) established a fueling protocol, J2601, for light-duty HFCEVs. It provides two fueling protocols for light-duty HFCEVs: (1) lookup table method and (2) MC formula method [20,21]. They are carried out at stations to control the fueling process within the pressure and temperature limits to ensure the fast filling of the vehicle within a given time frame [18].

This study presents the dynamic simulation for estimating fuel filling time for HFCEV from three high-pressure storage vessels (LP, MP, and HP banks) at different initial conditions. The SAE J2601 standard (lookup table method) was used to derive the fueling operation parameters, such as the station's target pressure and pressure tolerance, the APRR, and the initial estimated fueling time. A detailed heat transfer modeling suited for the process was discussed to correctly predict the in-cylinder temperature throughout the fueling operation. During the dynamic simulation, several parameters were checked to confirm the reliability of the process, such as the station pressure, the SOC%, the car tank temperature, the hydrogen flow rate, the amount of hydrogen gas accumulated

†To whom correspondence should be addressed.
E-mail: jhcho@kongju.ac.kr
Copyright by The Korean Institute of Chemical Engineers.

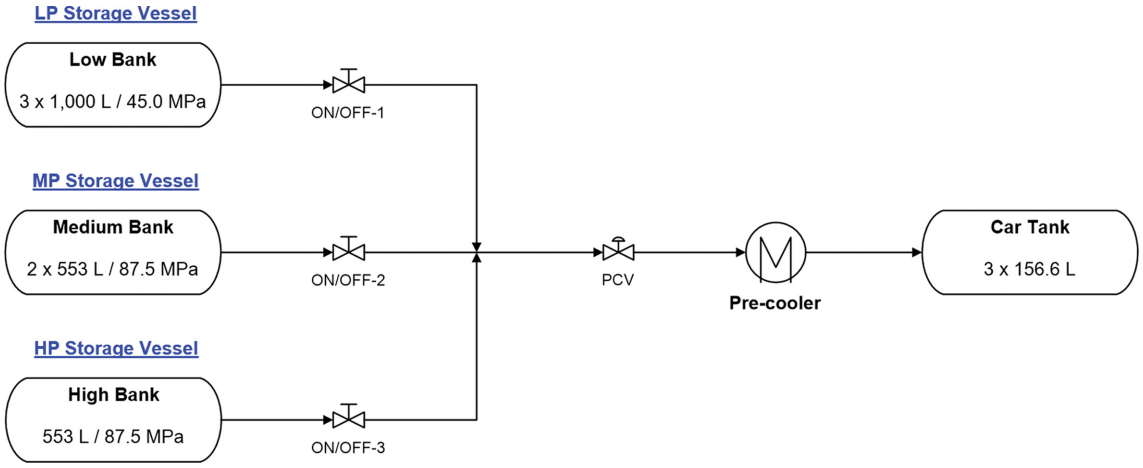


Fig. 1. Hydrogen trailer simplified process flow diagram.

Table 1. Vessel volume and initial operating conditions

Vessel name	Volume	Initial operating conditions
LP storage vessel (Low Bank)	1,000 L×3=3,000 L	45.0 MPa, ambient temperature
MP storage vessel (Medium Bank)	553 L×2=1,106 L	87.5 MPa, ambient temperature
HP storage vessel (High Bank)	553 L	87.5 MPa, ambient temperature
Car tank	52.2 L×3=156.6 L	Variable, ambient temperature

in the car tank, and the high-pressure storage vessel conditions. Finally, the fueling times calculated in the dynamic study were compared to their corresponding estimated values for all cases to confirm the integrity of the process.

HYDROGEN TRAILER CONFIGURATION

The overall process flow diagram shows the configuration of how the car tank will be pressurized using the three pressurized hydrogen fuel dispensers (LP, MP, and HP banks), as depicted in Fig. 1. Three different transfer processes are involved. First, the hydrogen gas will fill the car tank from the LP bank, followed by from the MP storage vessel, and finally from the HP storage vessel. The sequencing will be achieved with the aid of a 3-bank cascade configuration, wherein the on/off valves are strategically controlled to operate the transfer processes. Table 1 shows the vessels used for this study and their corresponding volume and initial operating conditions.

SAE J2601 was developed to ensure the fast filling of HFCEVs with 4-7 kg of hydrogen [20,21]. Due to the fast-fueling nature of the process, established performance and safety limits must be satisfied (Table 2). The maximum fuel filling rate of 60 g/s (3.6 kg/hr) should not be exceeded at any time during the process. The car tank's initial pressure should be at least 0.5 MPa or below the nominal working pressure of 70 MPa. The hydrogen gas temperature should be between −40 °C and 85 °C. The car hydrogen vessel is a type IV storage tank, and operating beyond the said temperature limits will degrade the tank liner. Dispensing the hydrogen gas at a fast rate increases the temperature of both the hydrogen and the tank liner. Thus, the hydrogen must be cooled to −40 °C before it is supplied to keep the car tank from exceeding its operating temperature (85 °C). If any of the said protocol limits are not satisfied, the fueling is terminated.

Table 2. SAE J2601 parameter limits for HFCEV fueling

Parameter	Limit value
Maximum flow rate	60 g/sec (3.6 kg/hr)
Hydrogen gas temperature	Min. −40 °C/Max. 85 °C
Dispenser pressure	Min. 0.5 MPa/Max. 87.5 MPa

1. Initial Fueling Time Estimation

The fueling time varies depending on the initial car tank pressure and ambient temperature. The initial estimated fueling time provides the approximate hydrogen filling time of the car tank for a given initial pressure (P_o) and ambient temperature (T_{amb}), excluding the non-fueling time. It can be used as an influential gauge for dynamic simulation and can be estimated using Eq. (1).

$$\text{Initial Estimated Fueling Time} = \frac{P_{Target} - P_0}{\text{APRR}} \quad (1)$$

The average pressure ramping rate (APRR) and target pressure (P_{Target}) can be determined using SAE J2601 look-up table (Fig. 2). For example, given a car tank with an initial pressure of 10 MPa and an ambient temperature of 20 °C, the APRR can be determined upon projecting the right-side value of the given ambient temperature. The target pressure can be located by getting the intersection of the row for ambient temperature and the column for car initial tank pressure on the table. For the given initial conditions, the APRR and target pressure are confirmed to be 21.8 MPa/min and 86.8 MPa, respectively, as highlighted in Fig. 2. The initial estimated

H70-T40 4-7 kg comm		APRR [MPa/min]	Target Pressure Ptarget [MPa]	Target Pressure Top-Off [MPa]	Top-Off APRR [MPa/min]	Target Pressure, Ptarget [MPa]											
			Initial Tank Pressure, P_o [MPa]														
			0.5-5 (no interpolation)			0.5	2	5	10	15	20	30	40	50	60	70	>70
Ambient Temperature, T_{amb} [°C]	>50	No Fueling								No Fueling							
	50	5.1	78.2	87.5	2.6	Top-Off Fueling		80.8	85.7	86.8	86.5	85.8	85.0	84.0	82.7	81.1	No Fueling
	45	8.1	76.3	87.5	4.0			81.1	86.9	86.6	86.2	85.3	84.3	83.0	81.6	79.7	
	40	11.5	73.2	87.5	5.4			81.1	86.9	86.4	85.9	84.7	83.5	82.0	80.3	78.3	
	35	12.4	72.9	87.5	5.6			81.2	86.9	86.4	85.9	84.7	83.4	81.9	80.2	78.2	
	30	15.3	70.6	87.5	6.6			81.0	86.8	86.3	85.6	84.3	82.8	81.2	79.4	77.2	
	25	18.5	69.0	87.4	7.2			81.0	86.8	86.4	85.4	83.8	82.2	80.4	78.5	76.1	
	20	21.8	67.9	87.4	7.6			81.2	86.8	85.9	85.1	83.3	81.5	79.6	77.5	75.1	
	10	28.0	66.3	87.4	9.0			81.2	86.8	85.7	84.7	82.6	80.5	78.3	76.1	73.4	
	0	28.5	No Top-Off Fueling			78.4	84.6	86.8	85.6	84.4	83.1	80.6	78.1	75.6	73.1		
	-10	28.5				82.2	87.1	86.4	85.2	84.0	82.8	80.4	77.9	75.4	72.9		
	-20	28.5				86.0	86.8	86.1	84.9	83.7	82.4	80.0	77.6	75.1	72.7		
	-30	28.5				86.8	86.5	85.7	84.5	83.3	82.1	79.6	77.2	74.9	72.5		
	-40	28.5				86.5	86.2	85.4	84.2	83.0	81.8	79.3	77.0	74.6	72.3		
	<-40	No Fueling															

Fig. 2. SAE J2601 look-up table for T40 station with H70 hose communications fueling a 4-7 kg capacity car tank [20,21]. The APRR and target pressure are highlighted for initial car tank pressure and ambient temperature of 10 MPa and 20 °C, respectively.

Table 3. List of dynamic simulation cases based on car tank initial conditions including the determined APRR, target pressure, and initial estimated fueling time based on SAE J2601 look-up table

Case no.	Car tank initial pressure (MPa)	Ambient temperature (°C)	APRR (MPa/min)	Target pressure (MPa)	Initial estimated fueling time (min)
1	5	40	11.5	81.1	6.62
2	5	30	15.3	81.0	4.97
3	5	20	21.8	81.2	3.50
4	5	10	28.0	81.2	2.72
5	5	0	28.5	86.8	2.87
6	5	−10	28.5	86.4	2.86
7	10	40	11.5	86.9	6.69
8	10	30	15.3	86.8	5.02
9	10	20	21.8	86.8	3.52
10	10	10	28.0	86.8	2.74
11	10	0	28.5	85.6	2.65
12	10	−10	28.5	85.2	2.64

fueling time of 3.52 minutes can be confirmed by applying Eq. (1). The APRR, target pressure, and initial estimated fueling time for different car tank initial conditions are summarized in Table 3. The twelve different cases based on car tank initial conditions will later be used as a basis for the dynamic simulation.

Top-off fueling protocol should be adopted for a car tank with initial pressures between 0.5 and less than 5 MPa at an ambient temperature above 0 °C. The top-off fueling initiates the filling at the same APRR as the non-communications fueling for the same boundary conditions up to an intermediate pressure. The APRR is then reduced until it approaches the top-off target pressure. For this study, the top-off fueling protocol will not be used as the car tank's initial pressure is set to either 5 MPa or 10 MPa.

2. SAE J2601 Fueling Corridor Pressure Tolerance

During the hydrogen fueling operation, the pressure of the dispenser attached to the car tank or the station pressure must fall within the pressure limits. The pressure limits can be easily visualized using Fig. 3. In this figure, the non-fueling time events, such as transferring of hydrogen source from one bank to another, are not included. The standard station pressure line connects the initial car tank pressure and the target pressure with APRR as the slope; all are determined using the SAE J2601 look-up table. As per SAE J2601, the upper and lower ΔP tolerances are 2.5 MPa and 7.0 MPa, respectively [20,21]. The upper pressure tolerance line is drawn parallel or the same slope as the standard station pressure line. The pressure will start from $P_o+\Delta P_{upper}$ to the target pressure.

Meanwhile, the lower pressure tolerance line is also drawn parallel to the standard station pressure line. The pressure will start from P_o, but will be constant until the standard station pressure is equal to $P_o+\Delta P_{lower}$. From that point, it will be projected to the target pressure. For common practice, the standard station pressure acts as the set pressure at a given time for the pressure control valve.

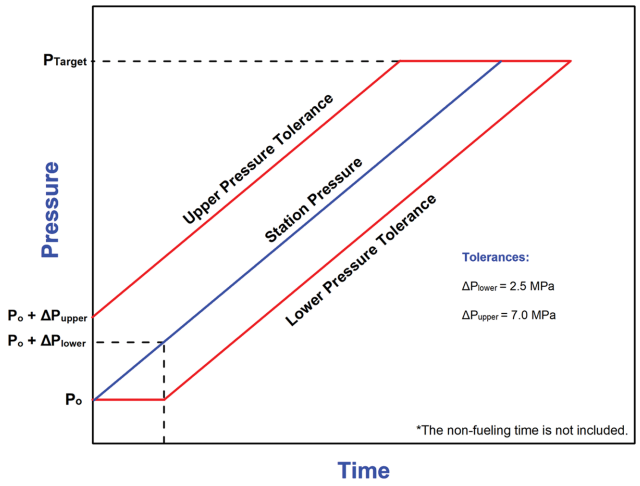


Fig. 3. SAE J2601 fueling corridor pressure tolerance.

However, the actual station pressure is set above the standard station pressure near the upper pressure tolerance line to speed up the hydrogen fueling operation for this study.

3. Pressure Control Valve Configuration

The pressure at the dispenser is controlled in the station to keep the desired APRR. The resulting APRR is anticipated to coincide within an allowed range, determined by the initial pressure, target pressure, and the fueling time elapsed. In the event that the APRR falls outside the limits, the hydrogen fueling process is halted. For the hydrogen flow rate monitoring, a mass flow meter (MFM) is located downstream of the pressure control valve.

The dispenser pressure is assigned as the set point pressure (P_{SP}) and derived from the look-up table. The P_{SP} is expressed as the sum of the initial car tank pressure and the product of the APPR and the fueling time elapsed (Eq. (2)).

$$P_{SP}=P_o+(\text{APRR})(\text{time elapsed}) \tag{2}$$

The control valve adjusts the process variable pressure close to the set point pressure by controlling the hydrogen gas flowing through the valve. Note that the set point pressure varies over time. Thus, it will be difficult to represent this varying set pressure in the dynamic simulation. Therefore, an alternative way should be applied in the simulation as proposed in Fig. 4.

Since the APRR should be constant over time, this parameter will be used as the new set point for the pressure control valve configuration. The process variable APRR ($APRR_{PV}$) can be evaluated by rearranging Eq. (2), as shown in Eq. (3). The term P is the instantaneous pressure of the dispenser at the time elapsed during the hydrogen fueling process.

$$\text{APRR}_{PV}=\frac{P-P_o}{\text{time elapsed}} \tag{3}$$

The fallback procedure is initiated when the pre-cooling temperature does not fall within the expected station type pre-cooling temperature range (i.e., from −40 °C to −33 °C). After which, a new lower pressure ramp rate is calculated. Generally, if the fallback procedure is not present when pre-cooling temperature abnormality occurs, the station will abort the fueling operation. However, the protocol allows a fallback APRR calculation procedure only once. It does not roll back to the initial ramp rate if the pre-cooling temperature later reaches a value uniform with the station type [18]. In this study, the fallback procedure is not included since the downstream temperature after the pre-cooler is assumed to be constant at −40 °C.

4. Heat Transfer Model for Car Tank

The heat transfer rate for the car tank with the ambient air temperature, which provides a reasonable estimate on the temperature rise inside a hydrogen fast-filled car tank, is best described by the works of Deymi-Dashtebayaz et al. [22]. Here, the initial filling process is numerically modeled to evaluate the heat transfer rate between the in-cylinder gas and the cylinder wall by developing a correlation for predicting the inner convective heat transfer coefficient. Then, with the help of the developed correlation, simultaneous thermodynamic modeling of the in-cylinder gas and cylinder wall is performed to predict the filling process's thermal characteristics with reasonable accuracy.

The heat released from the in-cylinder gas to the cylinder wall is expressed using Eq. (4):

$$\delta Q=U_i A_i(T_g-T_\infty) \tag{4}$$

where δQ, U_i, A_i, T_g, and T_∞ are the calculated heat release, overall heat transfer coefficient, cylinder internal surface area, in-cylinder gas temperature, and ambient temperature, respectively.

As shown in Fig. 5, the compressed hydrogen storage system

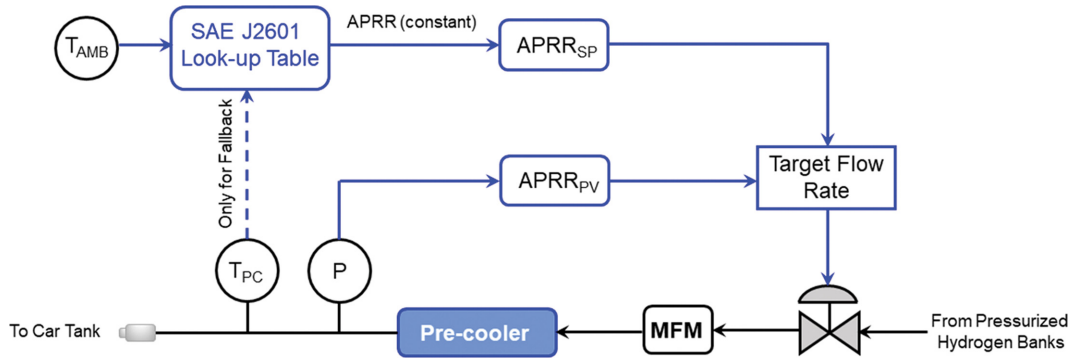


Fig. 4. Pressure control valve configuration.

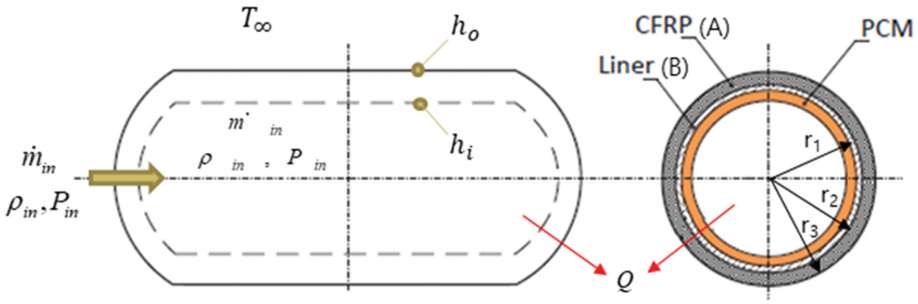


Fig. 5. A schematic diagram of hydrogen cylinder for heat transfer calculation.

(CHSS) used in this study is protected by three layers: (1) phase change material (PCM), (2) liner, and (3) carbon fiber-reinforced polymer (CFRP). These CHSS materials heavily affect the overall heat transfer coefficient. The U_i for a multi-layered wall with fluid flow on each side of the wall can be calculated using Eq. (5):

$$U_i = \frac{1}{\left[\frac{1}{h_i} + \frac{r_1}{k_A}\ln\left(\frac{r_2}{r_1}\right) + \frac{r_2}{k_B}\ln\left(\frac{r_3}{r_2}\right) + \frac{1}{h_o}\left(\frac{r_1}{r_3}\right)\right]} \quad (5)$$

where h_i is the in-cylinder gas convective heat transfer coefficient; h_o is the convective heat transfer coefficient at the cylinder wall; k_A and k_B are the thermal conductivities of the CHSS materials; r_1, r_2, and r_3 are the distance from the cylinder center to the CHSS material's surface for PCM, liner, and CFRP, respectively.

The in-cylinder gas convective heat transfer coefficient (h_i) can be determined using the definition of Nusselt (Nu) number (Eq. (6)):

$$Nu = \frac{h_i d}{k_g} \quad (6)$$

where d and k_g are the nozzle inlet diameter and the thermal conductivity for the in-cylinder hydrogen gas at its temperature, respectively. The correlation used for k_g is based on the Design Institute for Physical Properties (DIPPR). The DIPPR equation for hydrogen vapor thermal conductivity is presented in Eq. (7):

$$k_g = \frac{0.002653(T^{0.7452})}{1 + \frac{12}{T}} \quad (7)$$

where k_g is in W/m-K, and T is the in-cylinder hydrogen gas temperature in K.

The computation for the Nusselt number is adapted from elsewhere [22,23]. Based on the correlation, the Nusselt number is greatly dependent on ($\dot{m}_r$), which is defined as the ratio of the inlet mass flow rate ($\dot{m}_{in}$) and maximum mass flow rate ($\dot{m}_{max}$), as expressed in Eq. (8):

$$Nu = \begin{cases} 22512\dot{m}_r + 1163.4 & \dot{m}_r < 0.03 \\ 22358\dot{m}_r^{0.7184} & \dot{m}_r \geq 0.03 \end{cases} \quad (8)$$

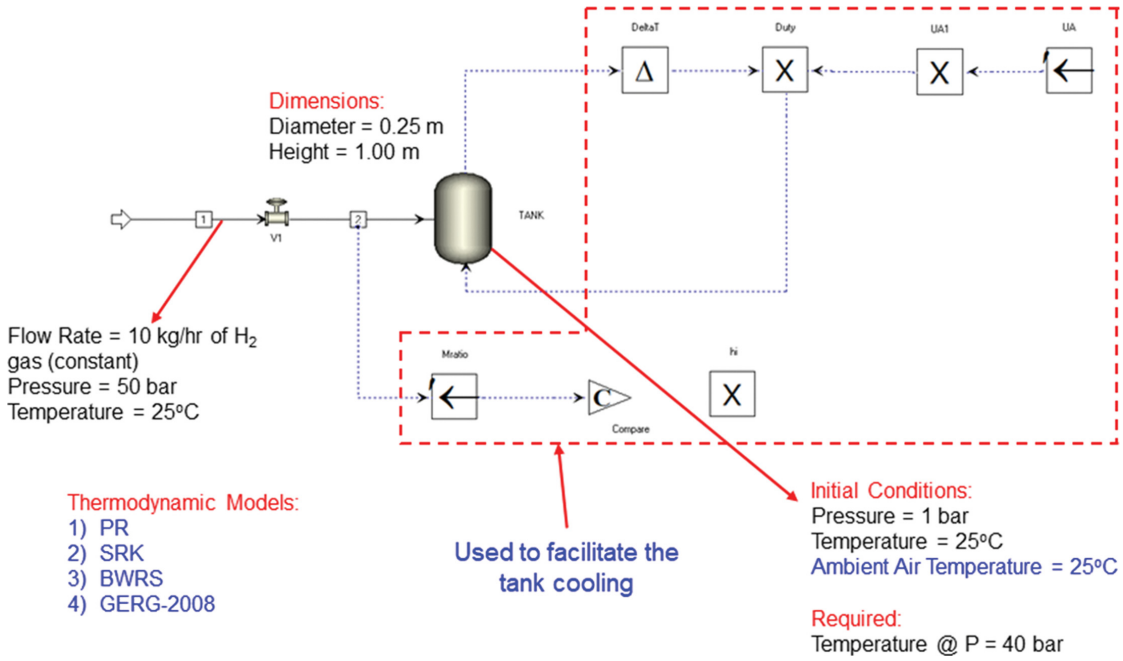


Fig. 6. Process flow diagram used for thermodynamic model comparison study in Aspen Dynamics.

Maximum flow rate ($\dot{m}_{max}$) happens in the choking condition and can be calculated using Eq. (9) [24]:

$$\dot{m}_{max} = A_N \sqrt{\gamma \rho_{in} P_{in} \left(\frac{2}{\gamma+1}\right)^{\frac{\gamma+1}{\gamma-1}}} \quad (9)$$

where A_N, γ, ρ_{in}, and P_{in} are inlet nozzle area, hydrogen specific ratio (C_p/C_v), density, and pressure of the hydrogen reservoir, respectively.

Note that the heat transfer model presented above is only applicable for the car tank. For the hydrogen dispenser vessels (LP, MP, and HP banks), the heat transfer mechanism is governed by depressuring that causes temperature-lowering inside the tank.

COMPARISON OF THERMODYNAMIC MODELS

An appropriate thermodynamic model suitable for hydrogen tank filling was first determined. Here, a simple comparison of several thermodynamic models, namely Peng-Robinson (PR), Soave-Redlich-Kwong (SRK), Benedict-Webb-Rubin-Starling (BWRS), and GERG-2008 equations of state, was used. Using several thermodynamic models, the time to fill hydrogen gas into a storage tank is estimated via process simulation and carried out using Aspen Dynamics v.11. As seen in Fig. 6, the study was facilitated by filling a vertical tank (with 2 : 1 ellipsoidal head, Diameter=0.25 m, Height=1.00 m) from initial conditions of $P_{Initial}$=1.0 bar and $T_{Initial}$= 25 °C to a final pressure of P_{Final}=40.0 bar. The tank was filled with hydrogen gas at a constant flow rate, pressure, and temperature (10 kg/hr of H_2 at P=50.0 bar & 25 °C) while the tank's heat transfer rate or cooling with the ambient air temperature was considered.

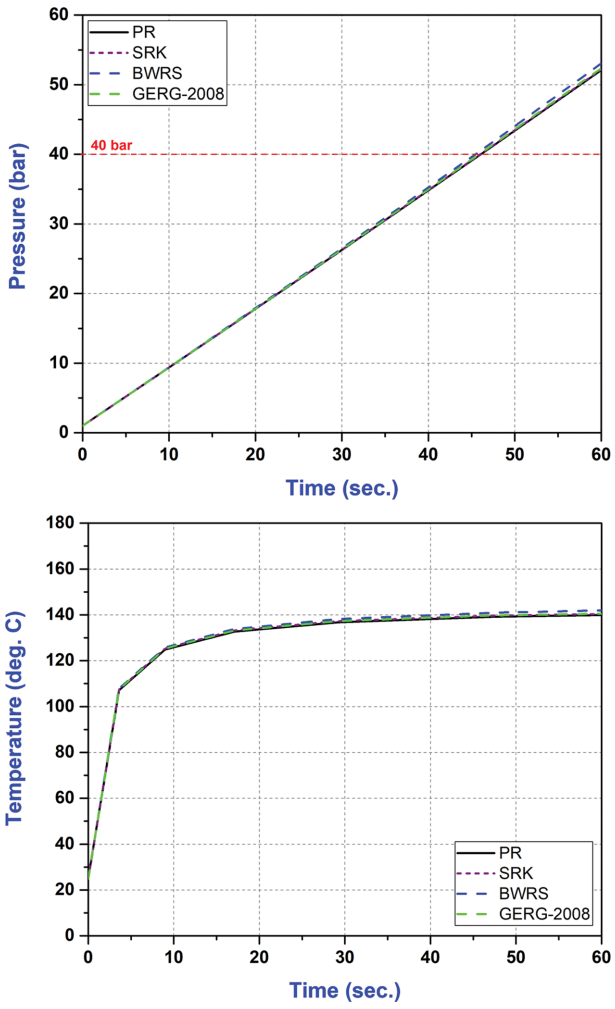


Fig. 7. Combined pressure and temperature profiles for hydrogen tank filling using several thermodynamic models.

Table 4. Tank filling time and final conditions using several thermodynamic models

Thermodynamic model	Final pressure (bar)	Temperature (°C)	Filling time (sec)
PR	40.0	139.991	46.080
SRK	40.0	139.464	46.008
BWRS	40.0	139.647	45.468
GERG-2008	40.0	139.541	45.864

As shown in Fig. 7 and Table 4, it takes around ~46 sec to pressurize the tank to a final pressure of 40.0 bar for all thermodynamic models. The corresponding temperatures were found out to be around ~140 °C. The results imply that the filling times for the different thermodynamic models have little to no significant differences from each other, proving that any of the used equations of state can be utilized for hydrogen gas filling modeling. However, the PR model gave the highest temperature and the longest filling time among the candidate models, making it more conservative. Therefore, PR was used as the thermodynamic model in this study.

DYNAMIC SIMULATION

The hydrogen fuel filling time for HFCEV at different initial conditions is estimated using dynamic simulation. In this study, the dynamic simulation was carried out using Aspen Dynamics v.11 with Peng-Robinson as the thermodynamic model. The simulation process was divided into three parts, in which the different storage vessels (LP, MP, and HP banks) act as the sole hydrogen source (Fig. 8). Initially, the steady-state simulation via Aspen Plus v.11 was set up and converted into dynamic ones. Thus, the control valve was sized to provide sufficient pressure drop with the valve half-open. In the steady-state simulation, the hydrogen flow rate passing through the control valve was set to 50% of the maximum allowable flow rate (50% of 60 g/sec=30 g/sec) since the default opening of the valve was 50% once converted into a dynamic file. The sizes of the vessels are based on the total volume provided in Table 1. The tanks are vertical with a 2 : 1 ellipsoidal head and a fixed length to diameter ratio of 2. The initial conditions of the vessels are given in Tables 1 and 3, in which 12 different cases are presented. Finally, the steady-state flowsheets were pressure checked, and Aspen Plus files exported to Aspen Dynamics as pressure-driven simulations.

A conventional proportional-integral (PI) controller was utilized to manipulate the pressure control valve wherein the process vari-

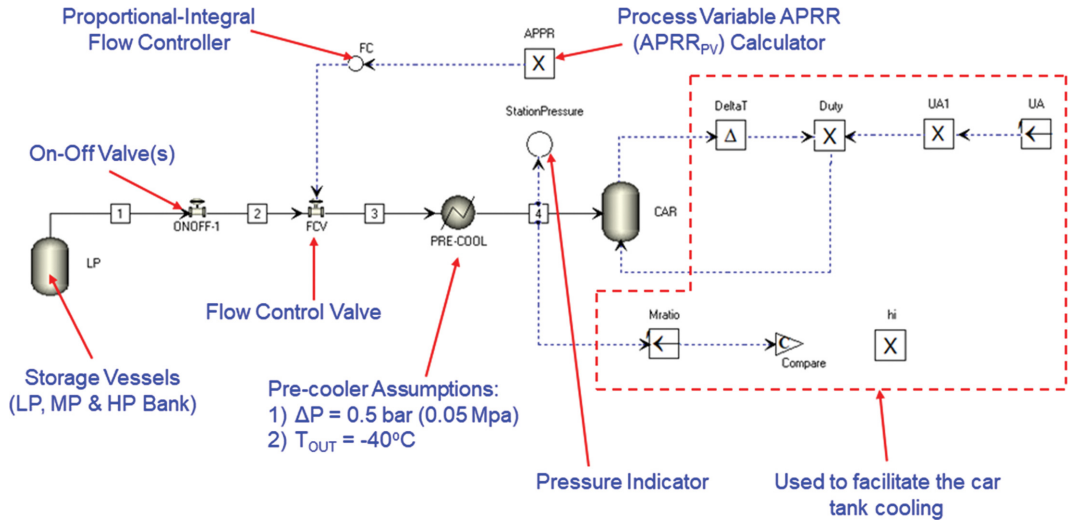


Fig. 8. Process flow diagram (main study) in Aspen Dynamics.

Table 5. Parameter values used for car tank heat transfer calculations

Parameter	Symbol	Value
Cylinder internal surface area	A_i	0.8 m^2
Thermal conductivities of CHSS materials	k_A, k_B	0.5 W/m-K
Convective heat transfer coefficient at the cylinder wall	h_o	5 W/m^2-K
Distance from the cylinder center to the PCM's surface	r_1	270 mm (0.270 m)
Distance from the cylinder center to the liner's surface	r_2	275 mm (0.275 m)
Distance from the cylinder center to the CFRP's surface	r_3	310 mm (0.310 m)
Nozzle inlet diameter	d	5 mm (0.005 mm)
Specific ratio	γ	1.4

able APRR was adjusted close to the set point APRR. The proportional gain and the integral time used are 10 and 0.1 min, respectively. For the pre-cooler, the pressure drop was assumed to be 0.5 bar at maximum hydrogen flow. At the same time, the heat exchanger outlet temperature was preferred to be constant at −40 °C to keep the temperature, especially the car tank, within limits once fast filling is in operation.

The pressure of the dispenser attached to the car tank (station pressure) is represented in the simulation as stream number 4. At the start of hydrogen fuel operation, the pressure control valve is closed. Therefore, the initial pressure at the dispenser is similar to that of the car tank's initial pressure since the pressure drop between the station pressure and the car tank is assumed to be negligible. For the car tank heat transfer, a series of control logics are used to represent the mechanism. In addition, the flow sheet box in Aspen Dynamics is utilized, incorporating Eq. (4) to Eq. (9). The fixed parameter values used for the heat transfer calculations are shown in Table 5.

1. Hydrogen Fuel Filling Checkpoints

During and after the course of the hydrogen fuel filling via dynamic simulation, several parameters should be checked to confirm the reliability of the process. First, the calculated station pressure should fall within the pressure limits at any time. The state of charge (SOC%), which measures the fuel filling percentage of the car tank, should be more than 95% after filling. The SOC% can be calculated using Eq. (10):

$$\text{SOC}(\%) = \frac{\text{Density at temperature \& pressure condition after fuel fillin}}{\text{Density at 15 °C \% 70 MPa (40.2 g/L)}} \times 100\% \quad (10)$$

The temperature of the compressed hydrogen inside the car tank after fuel filling must be below the maximum allowable temperature of 85 °C for Type IV vessels. At any given time, the hydrogen flow rate should peak not more than 60 g/sec. Also, the amount of hydrogen gas accumulated in the car tank should be monitored. Lastly, the storage vessels' (hydrogen dispensers) conditions should be reported at the end of the fueling process.

2. Hydrogen Fuel Filling Procedure

Dynamic simulation for the hydrogen fuel filing of the car tank is divided into three stages. It starts with the LP bank supplying hydrogen gas to the car tank. Once the hydrogen transfer from the LP bank is completed, all of the conditions for the car tank are then carried over for the next stage, which is the hydrogen pressurization of the car tank from the MP bank. The MP bank is now used to fill the car tank. Similarly, at the end of the fueling process from the MP bank, the entire process conditions of the car tank are reflected in the last part of the simulation. Finally, the HP bank is utilized to complete the high-pressure compression of hydro-

gen gas into the car tank. Note that the pressure control valve opening is initially set to 0% at the start of every stage.

The filling operation from a storage vessel to the car bank will stop when (1) For LP and MP bank, the station pressure is below the limit; or when the mass flow rate becomes less than 10 g/s to ensure a fast filling rate. (2) For HP bank, the station pressure is below the limit; or when the pressure difference between the storage vessel and car bank becomes less than 10 bars (1.0 MPa); or when the SOC% approached 100%.

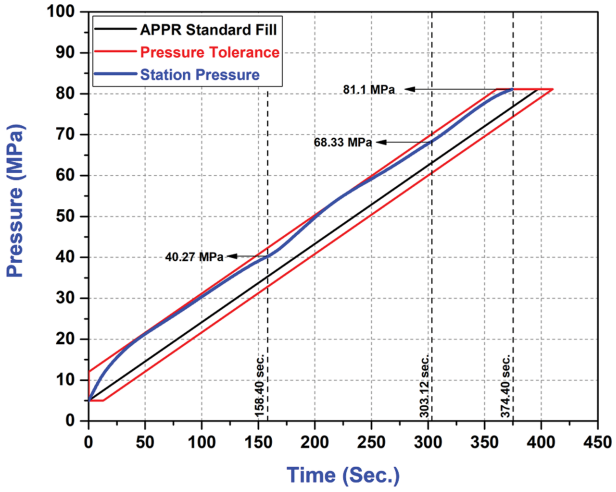
RESULTS AND DISCUSSION

The analysis and simulation to estimate the time for the hydrogen fuel filling of HFCEV from three high-pressure vessels at different initial conditions were performed using Aspen Dynamics v.11. A time step of 10^{-4} sec was used to ensure the reliability of the process. The fueling phase considered started from the main fueling phase, with non-fueling events being excluded. Twelve cases were analyzed wherein each had different vessel initial conditions (Tables 1 and 3). However, only cases 1 and 6 are discussed here since the two constitute the extreme temperatures (40 and −10 °C, respectively) for the car tank with an initial pressure of 5 MPa. The results for other cases are presented in the supplementary material file. Simulation results showing the different hydrogen fuel filling checkpoints such as the station pressure, SOC%, car tank temperature, hydrogen mass flow rate, car tank hydrogen content, and storage vessels' conditions (all vs. time) are summarized and discussed.

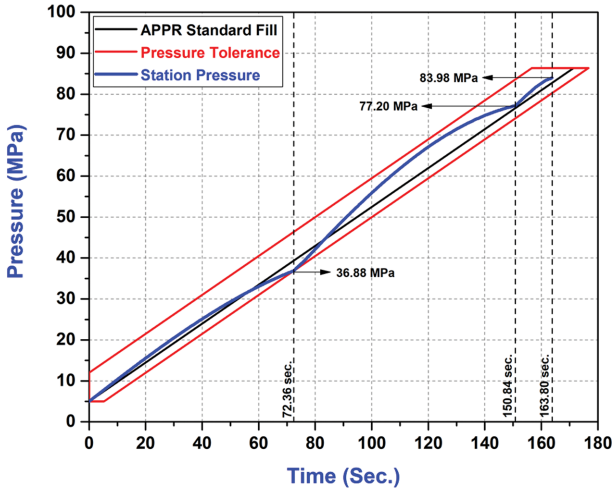
1. Station Pressure

The simulation results depicting the change in the station pressure vs. time are shown in Fig. 9. The station pressure is controlled in such a way that the calculated values through time should be near but not exceeding the upper pressure tolerance line. It is best demonstrated in case 1, where after ~25 sec, the station pressure is already close to the upper pressure limit. However, the trend is not similar in case 6 because the required APRR is higher.

The target pressures for cases 1 and 6 are 81.10 MPa and 86.40 MPa, respectively. Based on the results, only case 1 reached the target pressure. For case 6, the simulation stopped when the station pressure became 83.98 MPa since 100% SOC was already attained. The calculated fueling time needed to fill the car tank with hydro-

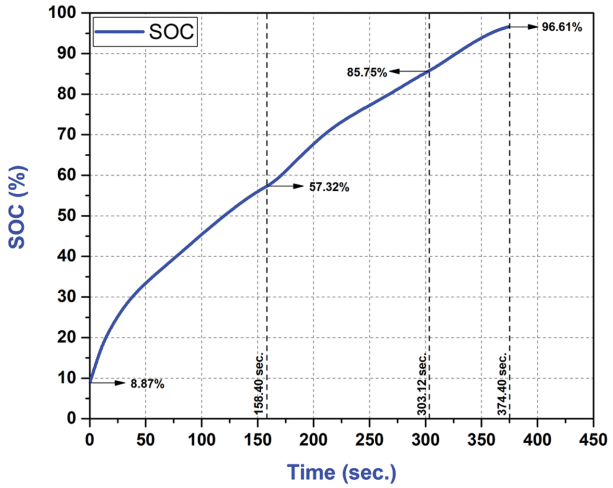


(a) Case 1

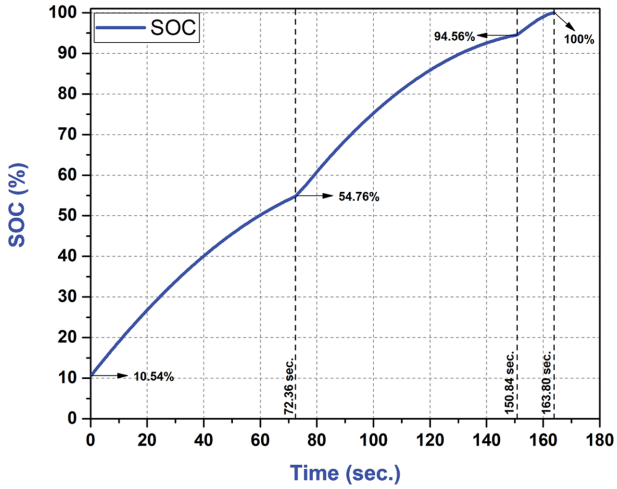


(b) Case 6

Fig. 9. Station pressure vs. time.



(a) Case 1



(b) Case 6

Fig. 10. State of charge (SOC) % vs. time.

gen gas from LP, MP, and HP banks was determined to be 374.40 sec (6.24 min) for case 1 and 163.80 sec (2.73 min) for case 6. The calculated fueling times are faster than the initially estimated values of 6.62 min and 2.86 min for cases 1 and 6, respectively. The station pressure and the car tank pressure have the same value since the pressure drop between them was assumed to be negligible.

2. SOC%

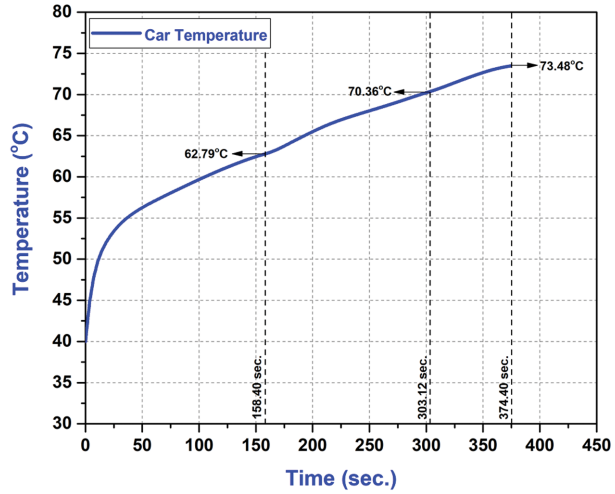
The measurement that tells the hydrogen fuel filling condition in terms of percentage is expressed using the state of charge (SOC%). The SOC% was calculated as defined in Eq. (10). In Fig. 10, the graphs of the SOC% over the hydrogen fueling time elapsed are illustrated. For case 1, the initial SOC% was 8.87%, then became 96.61% after filling. For case 6, the SOC% increased from 10.54% to 100% after completing the fueling process. The determined final SOC% for both cases satisfies the required value of greater than 95%.

3. Car Tank Temperature

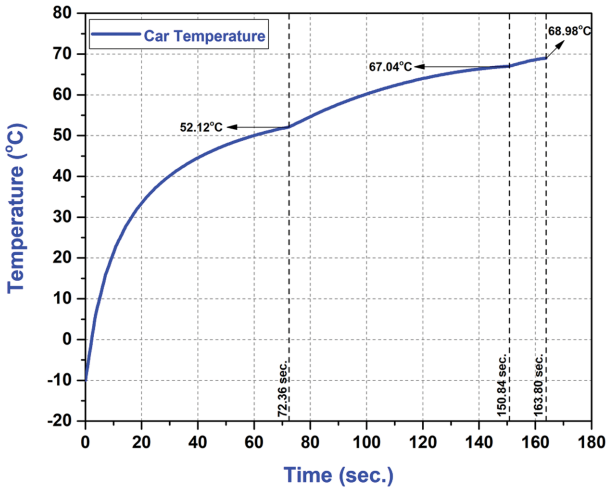
The maximum allowable working temperature for Type IV storage tanks is 85 °C. HFCEVs or the car hydrogen vessels, which are type IV storage tanks, should not operate beyond the temperature limits to avoid degrading the tank liner. The fast fueling of the car tank causes an abrupt increase in the temperature of the compressed hydrogen gas inside the vehicle vessel. As seen in Fig. 11, the car temperature increased dramatically in the first 30 seconds of the operation or when the hydrogen source originated from the LP bank for both cases. At the end of fueling, the car tank's final temperature was calculated to be at 73.48 °C for case 1 and 68.98 °C for case 6, both lower than the limit.

4. Hydrogen Mass Flow Rate

The hydrogen mass flow rate at the dispenser was monitored, and the trend is presented in Fig. 12. For case 1, a sudden increase of flow rate, which peaked at 56.71 g/sec, was observed in the first few seconds of the process. The immediate flow rate surge was associated with the station pressure being controlled to approach the upper pressure limit. It was made possible due to the fast action of the pressure control valve. When the car tank was pressurized by the MP and HP banks, only moderate hydrogen flow rates were needed to maintain the proximity of the station pressure from the upper limit. During the end of fueling from the LP and MP banks, the calculated pressure values were close enough to the limit, mak-

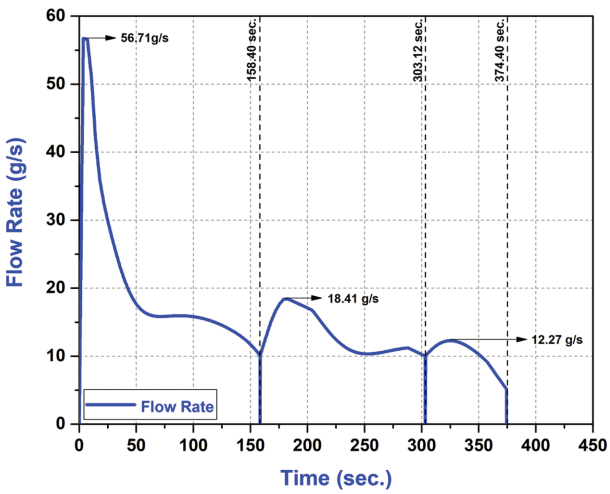


(a) Case 1

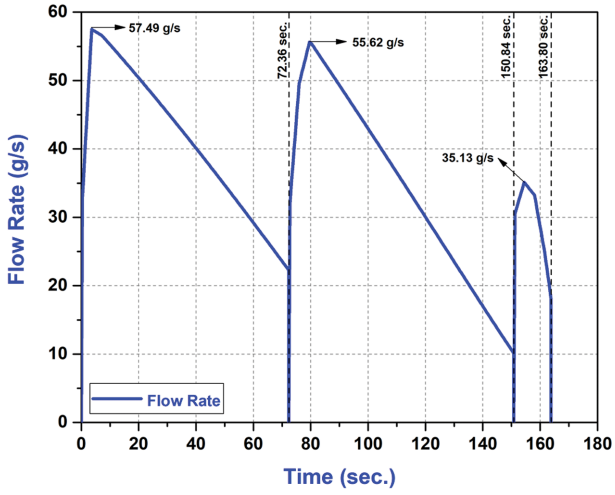


(b) Case 6

Fig. 11. Car tank temperature vs. time.

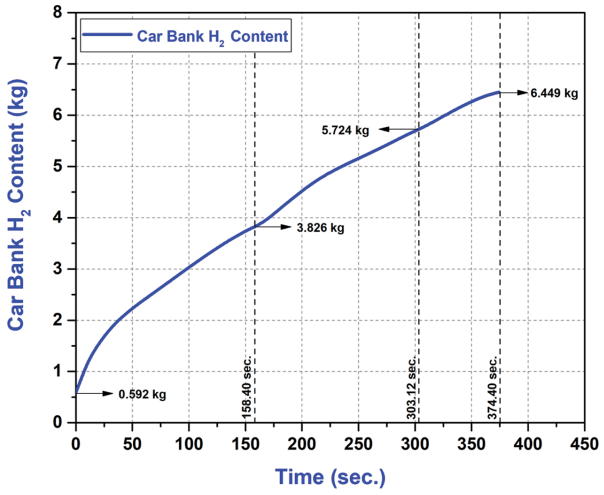


(a) Case 1

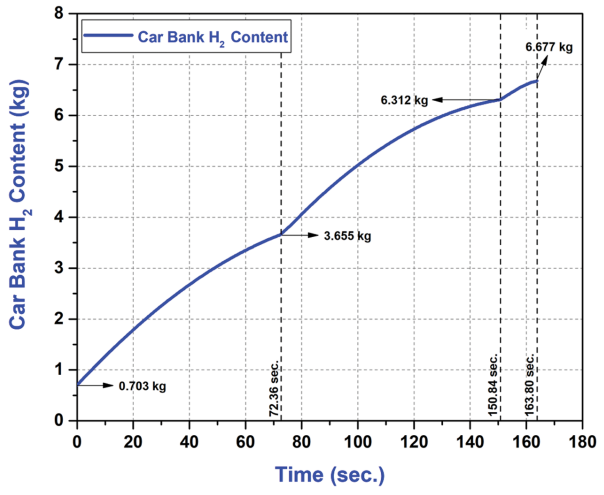


(b) Case 6

Fig. 12. Hydrogen mass flow rate vs. time.



(a) Case 1



(b) Case 6

Fig. 13. Car tank hydrogen content vs. time.

ing the control valve open moderately.

On the other hand, for case 6, it was observed that the flow rate built up at the start of every fueling process from the different banks. The rapid rise was linked to the control of station pressure by the pressure control valve. After which, the flow rate declined in a smooth straight line, suggesting that the control valve opening was maintained. Despite the valve opening remaining constant after the flow rate peaked, the rate of the hydrogen gas transfer decreased due to the reduced pressure gradient between the banks and the car tank, which is the main driving force for the hydrogen gas to be compressed in the car tank.

5. Car Tank Hydrogen Content

HFCEVs containing 4-7 kg of hydrogen gas were used as the basis for the lookup table for communications fueling in this study. As seen in Fig. 13, the hydrogen gas mass content inside the car tank is 6.449 kg for case 1, while 6.677 kg for case 6. Both values are within the mass range intended for the size of the car tank used for this study. The hydrogen content in case 6 was expected to be higher than that of case 1 since the SOC% achieved was higher.

6. Storage Vessels Conditions

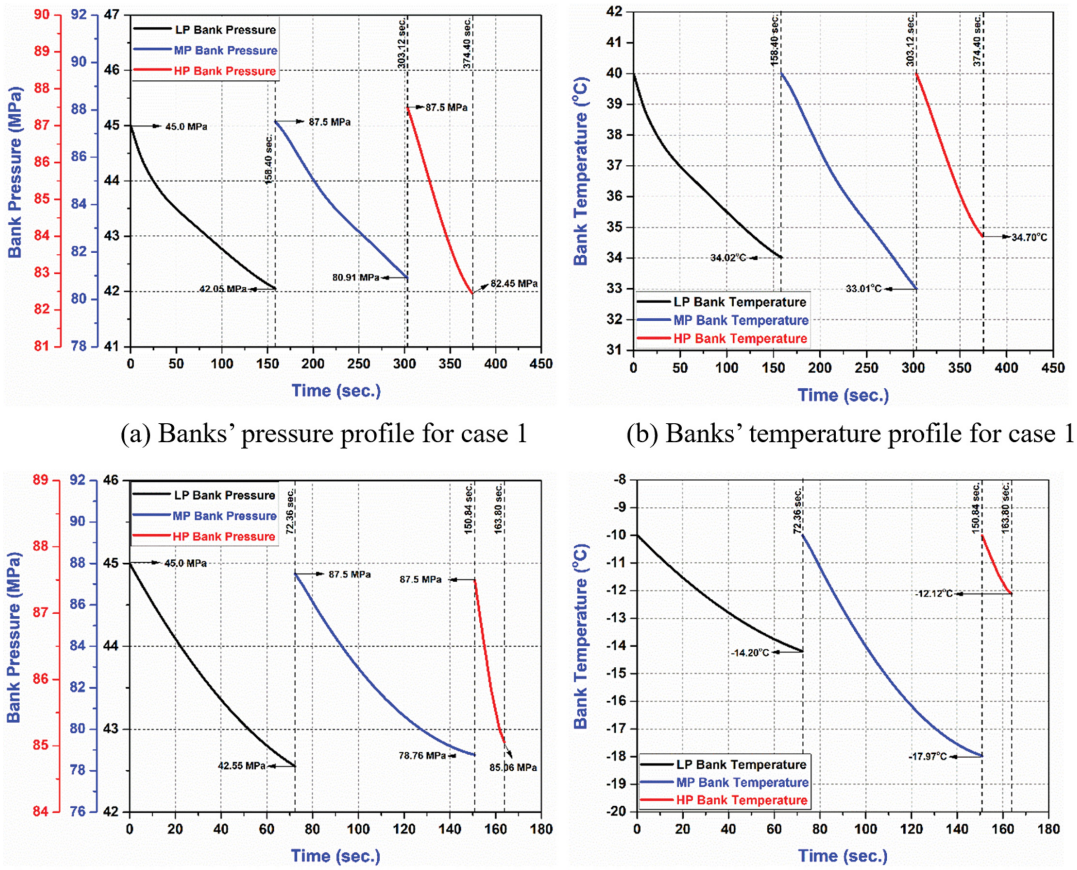
Storage vessels, namely the LP, MP and HP banks, were used to fill the car tank with compressed hydrogen gas. The pressure and temperature profiles for the two cases are shown in Fig. 14. As predicted, the pressure and the temperature decreased for all the banks. Since the tanks were the supplier of the hydrogen gas, the banks pressure were expected to be diminished during the fueling process. Meanwhile, the decline in banks temperature was the result of the tank depressuring effect.

7. Overall Summary of Dynamic Simulation Results

The overall dynamic simulation results for different cases are summarized in Table 6. Here, the calculated fueling time, station, or car tank pressure, SOC%, car tank temperature, and car tank are reported. All of the values are based on the end of the hydrogen fueling of the car tank. By comparing the calculated fueling time with the initial estimate in Table 3, it was observed that the fueling times calculated in the dynamic study were faster than their corresponding estimated value for all cases. For the station pressure/car tank pressure, cases 1 to 4 achieved their respective target pressure. The others almost approached their assigned target pres-

Table 6. Overall summary of dynamic simulation results for different cases

Case no.	Calculated fueling time (min)	Station pressure/ Car tank pressure (MPa)	SOC%	Car tank temperature (°C)	Car tank H_2 content (kg)
1	6.24	81.10	96.61	73.48	6.449
2	4.75	81.00	96.77	72.53	6.460
3	3.41	81.20	97.15	71.64	6.485
4	2.68	81.20	97.34	70.58	6.498
5	2.77	83.95	99.75	70.16	6.658
6	2.73	83.98	100	68.98	6.677
7	5.80	81.36	97.16	71.92	6.486
8	4.60	84.09	99.72	70.82	6.657
9	3.23	83.98	100	68.93	6.678
10	2.60	83.38	100	66.75	6.678
11	2.51	82.82	100	64.38	6.678
12	2.46	82.17	100	61.87	6.678



(a) Banks' pressure profile for case 1

(b) Banks' temperature profile for case 1

(c) Banks' pressure profile for case 6

(d) Banks' temperature profile for case 6

Fig. 14. Storage vessel conditions vs. time.

sure, but fueling ended since they either maxed the SOC% or reached the lowest pressure difference with the HP bank (ΔP=1.0 MPa). All of the reported SOC% were greater than the required (95%), and all of the car tank temperatures at the end of the filling process were less than the maximum allowable temperature of 85 °C. Finally, the car tank's final hydrogen gas content for all cases was within the basis (4-7 kg).

CONCLUSION

Analysis and dynamic simulation for estimating fuel filling time for HFCEV from three high-pressure storage vessels (LP, MP, and HP banks) at different initial conditions has been presented. SAE J2601 standard was used as the basis for the fueling operation where the station's target pressure and its pressure tolerance, the APRR, and the initial estimated fueling time were derived. The pressure control valve with PI controller was utilized in such a way that the process variable APRR approached the set APRR. For the fast filling of the car tank with hydrogen gas, a detailed heat transfer modeling suited for the process was elaborated to correctly predict the in-cylinder temperature throughout the course of the fueling operation. During the dynamic simulation, several parameters were checked to confirm the reliability of the process, such as the station pressure, the SOC%, the car tank temperature, the hydrogen flow rate, the amount of hydrogen gas accumulated in the car tank, and the high-pressure storage vessel conditions. All of which were monitored and confirmed to be according to their expected values or limits. Lastly, the fueling times calculated in the dynamic study were faster than their corresponding estimated values for all cases, indicating the integrity of the process.

ACKNOWLEDGEMENT

This work is supported by the "R&D Center for Reduction of Non-CO_2 Greenhouse gases" (2017002410009) funded by Korea Ministry of Environment (MOE) as Global Top Environment R&D Program.

CONFLICT OF INTEREST

The authors declare that there is no conflict of interest regarding the publication of this manuscript.

SUPPORTING INFORMATION

Additional information as noted in the text. This information is available via the Internet at http://www.springer.com/chemistry/journal/11814.

REFERENCES

1. B. Johnston, M. C. Mayo and A. Khare, *Technovation*, **25**, 569 (2005).
2. J.-Q. Li, N.-S. Myoung, J.-T. Kwon, S.-J. Jang and T. Lee, *Energies*, **13**(23), 6428 (2020).
3. J.-Q. Li, J.-C. Li, K. Park, S.-J. Jang and T. Lee, *Energies*, **14**(9), 2635 (2021).
4. Y. Ma, X. R. Wang, T. Li, J. Zhang, J. Gao and Z. Y. Sun, *Int. J. Hydrogen Energy*, **46**(54), 27330 (2021).
5. M. Nagpal and R. Kakkar, *Int. J. Hydrogen Energy*, **43**(27), 12168 (2018).
6. N. Sazali, *Int. J. Hydrogen Energy*, **45**(38), 18753 (2020).
7. J. O. Abe, A. P. I. Popoola, E. Ajenifuja and O. M. Popoola, *Int. J. Hydrogen Energy*, **44**(29), 15072 (2019).
8. D. Mori and K. Hirose, *Int. J. Hydrogen Energy*, **34**(10), 4569 (2009).
9. M. Li, Y. Bai, C. Zhang, Y. Song, S. Jiang, D. Grouset and M. Zhang, *Int. J. Hydrogen Energy*, **44**(21), 10677 (2019).
10. D. J. Han, K. R. Bang, H. Cho and E. S. Cho, *Korean J. Chem. Eng.*, **37**(8), 1306 (2020).
11. S. M. A. A. Ibrahim, *Korean J. Chem. Eng.*, **31**, 1792 (2014).
12. T. W. Kim, C. Kim, H. Jeong, C. H. Shin and Y. W. Suh, *Korean J. Chem. Eng.*, **37**(8), 1427 (2020).
13. S. E. Moradi, *Korean J. Chem. Eng.*, **31**(9), 1651 (2014).
14. S. U. Rather, *Korean J. Chem. Eng.*, **33**(5), 1551 (2016).
15. R. Krishna, E. Titus, M. Salimian, O. Okhay, S. Rajendran, A. Rajkumar, J. M. G. Sousa, A. L. C. Ferreira, J. C. Gil and J. Gracio, *Hydrogen storage for energy application,* In *Hydrogen storage,* IntechOpen (2012).
16. T. Johnson, R. Bozinoski, J. Ye, G. Sartor, J. Zheng and J. Yang, *Int. J. Hydrogen Energy*, **40**(31), 9803 (2015).
17. D. Chapelle and D. Perreux, *Int. J. Hydrogen Energy*, **31**(5), 627 (2006).
18. K. Reddi, A. Elgowainy, N. Rustagi and E. Gupta, *Int. J. Hydrogen Energy*, **42**(26), 16675 (2017).
19. B. Tanç, H. T. Arat, E. Baltacıoğlu and K. Aydın, *Int. J. Hydrogen Energy*, **44**(20), 10120 (2019).
20. Society of Automotive Engineers (SAE), *Fueling Protocols for Light Duty Gaseous Hydrogen Surface Vehicles (Standard J2601_201407),* SAE International (2014).
21. Society of Automotive Engineers (SAE), *Fueling Protocols for Light Duty Gaseous Hydrogen Surface Vehicles (Standard J2601_201612),* SAE International (2016).
22. M. Deymi-Dashtebayaz, M. Farzaneh-Gord, N. Nooralipoor and H. Niazmand, *Brazilian J. Chem. Eng.*, **33**, 391 (2016).
23. M. Deymi-Dashtebayaz, M. Farzaneh-Gord, N. Nooralipoor and S. Rastgar, *J. Nat. Gas Sci. Eng.*, **21**, 1099 (2014).
24. P. H. Oosthuizen and W. E. Carscallen, *Compressible fluid flow*, McGraw-Hill (1997).

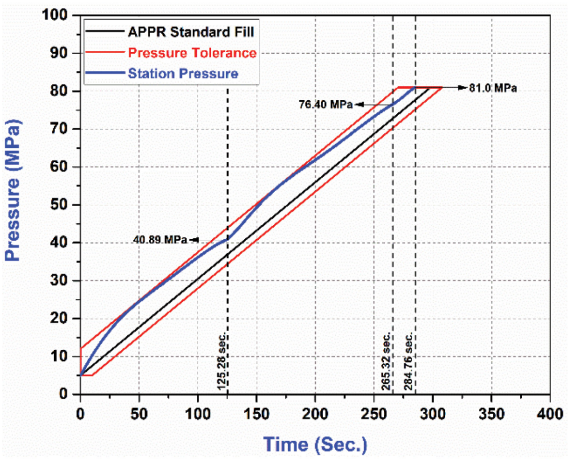
Supporting Information

Fuel filling time estimation for hydrogen-powered fuel cell electric vehicle at different initial conditions using dynamic simulation

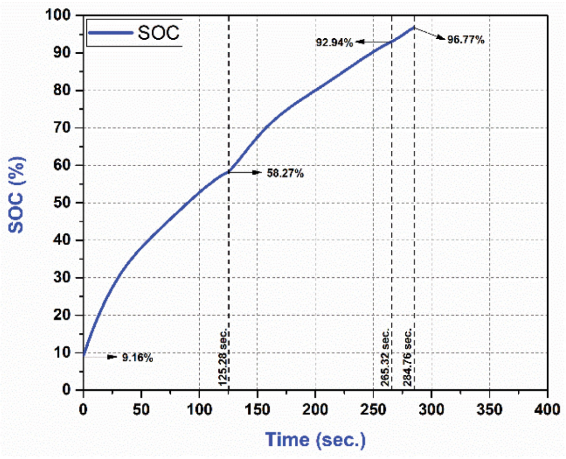
Russel J. Galanido*, Leah Jessica Sebastian*, Daniel Owusu Asante*, Dong Sun Kim*, Nam-Ju Chun, and Jungho Cho*,†**

*Chemical Process Research Laboratory, Department of Chemical Engineering, Kongju National University, 275 Budae-dong, Cheonan-si, Seobuk-gu, Chungcheongnam-do 31080, Korea
**NK CO., LTD, 194-11, Gwahaksandan-ro, Gangseo-gu, Busan 46743, Korea
(*Received 12 July 2021 • Revised 10 October 2021 • Accepted 13 October 2021*)

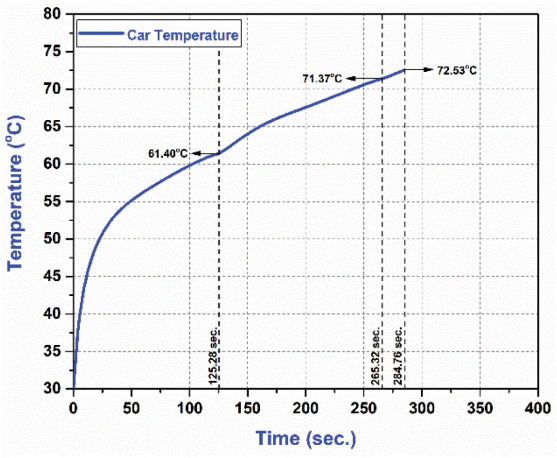
Case 2: 5.0 MPa, 30 °C



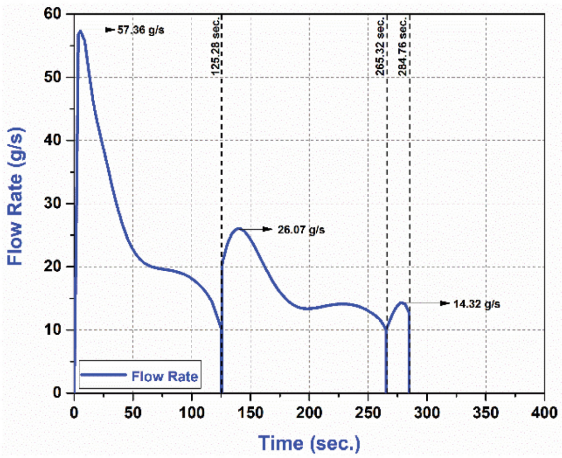
(a) Station pressure vs. time.



(b) State of charge (SOC) % vs. time.

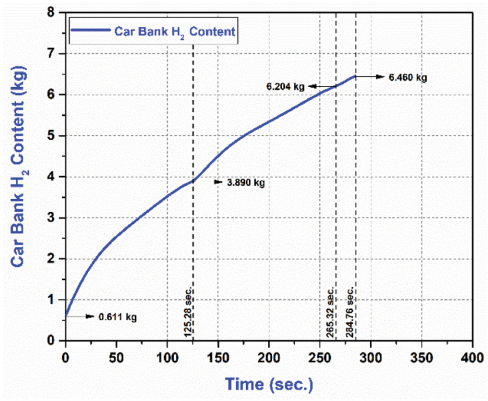


(c) Car tank temperature vs. time.

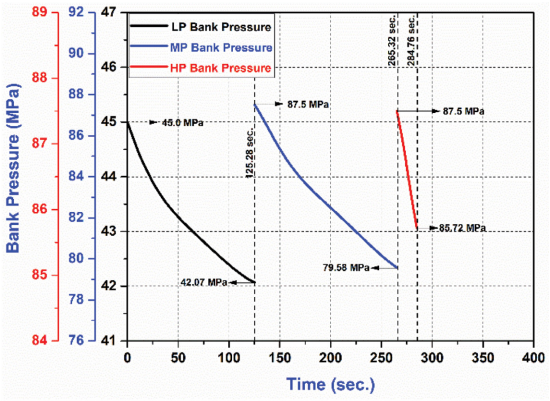


(d) Hydrogen mass flow rate vs. time.

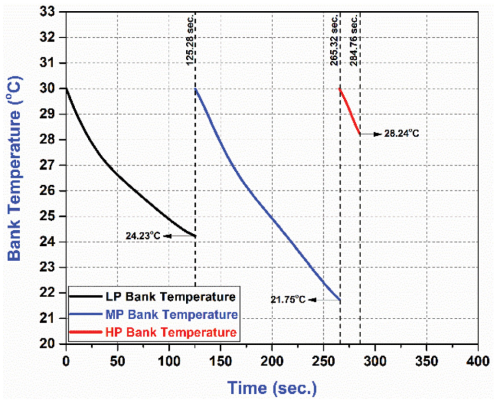
Fig. S1. Case 2 checkpoints results vs. time.



(e) Car tank hydrogen content vs. time.



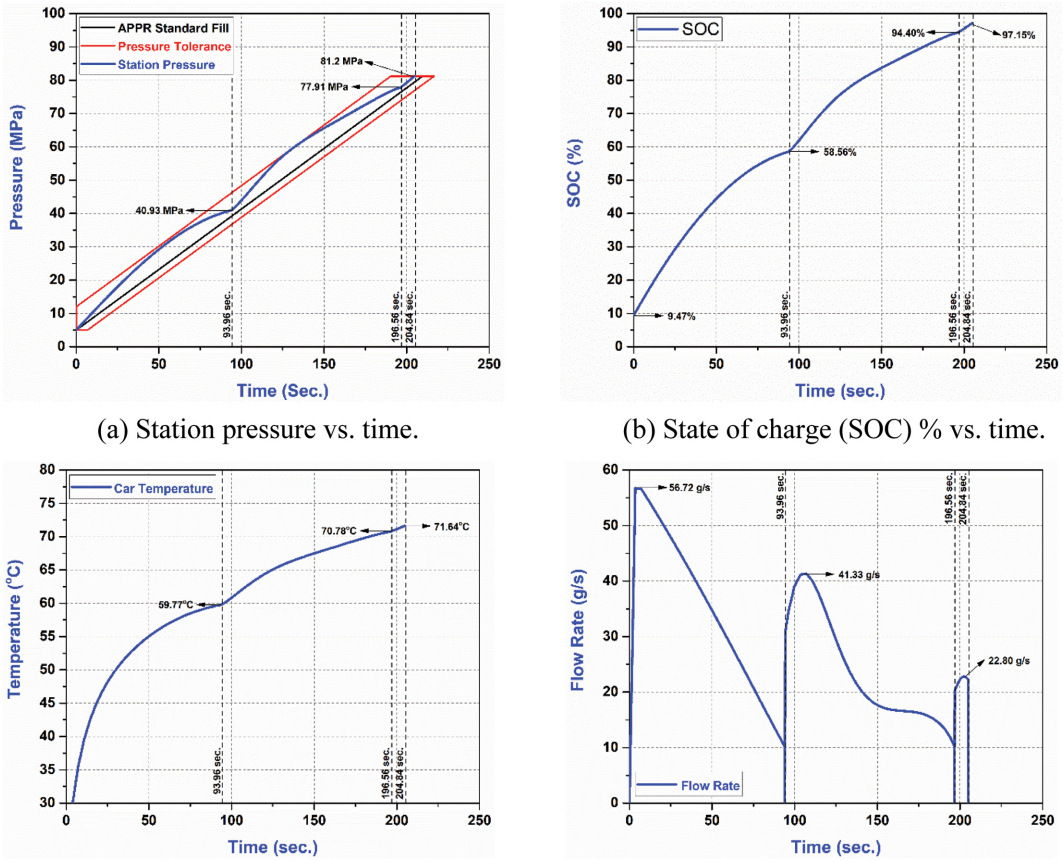
(f) Banks' pressure profile.



(g) Banks' temperature profile.

Fig. S1. Continued.

Case 3: 5.0 MPa, 20 °C



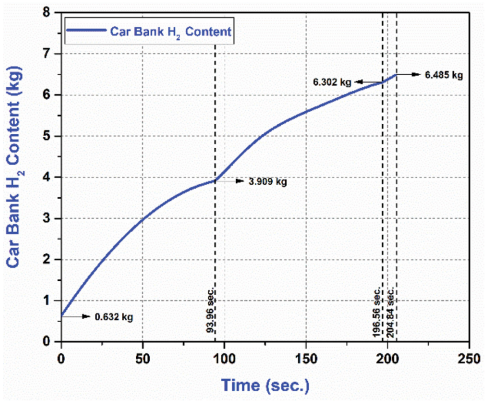
(a) Station pressure vs. time.

(b) State of charge (SOC) % vs. time.

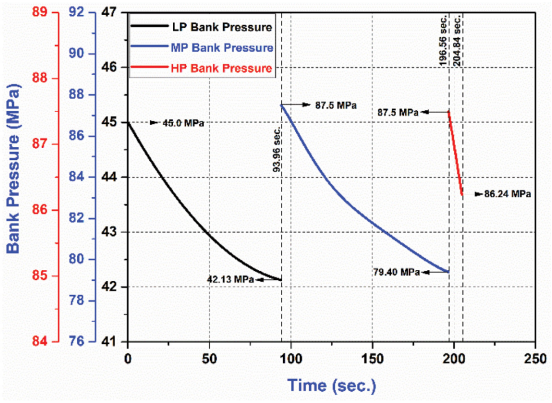
(c) Car tank temperature vs. time.

(d) Hydrogen mass flow rate vs. time.

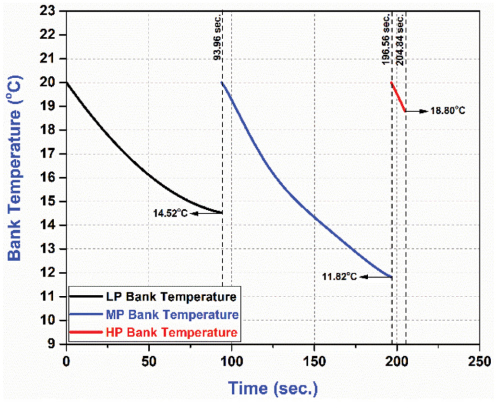
Fig. S2. Case 3 checkpoints results vs. time.



(e) Car tank hydrogen content vs. time.



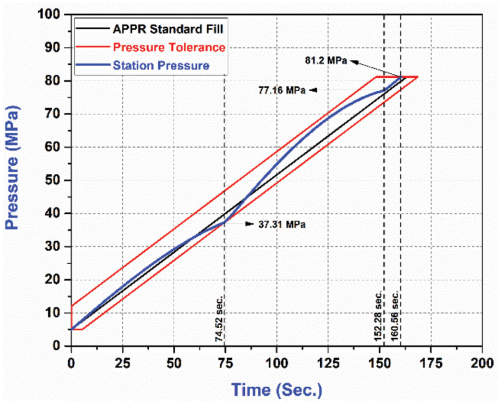
(f) Banks' pressure profile.



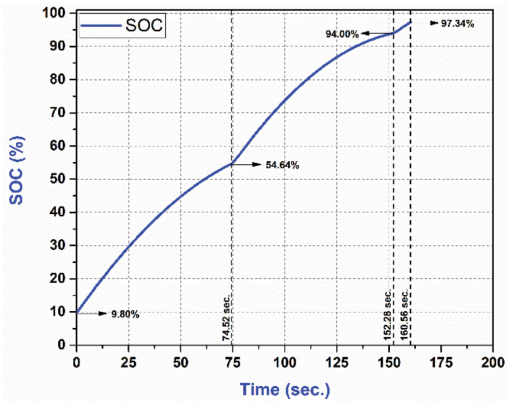
(g) Banks' temperature profile.

Fig. S2. Continued.

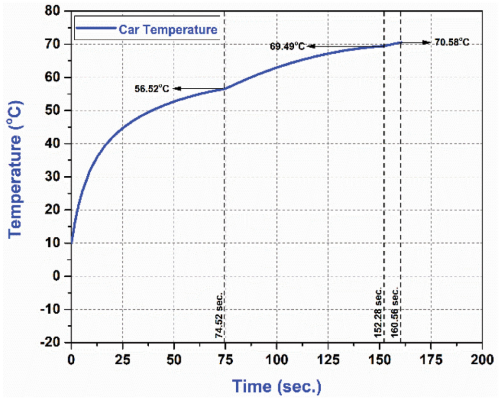
Case 4: 5.0 MPa, 10 °C



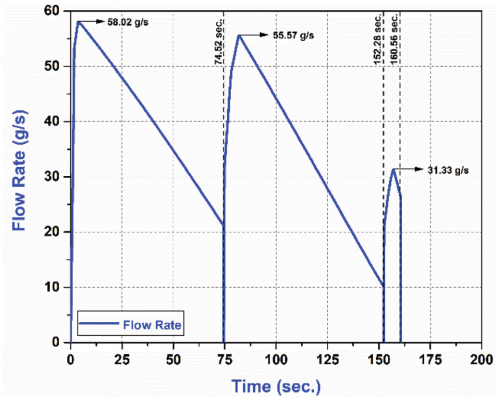
(a) Station pressure vs. time.



(b) State of charge (SOC) % vs. time.

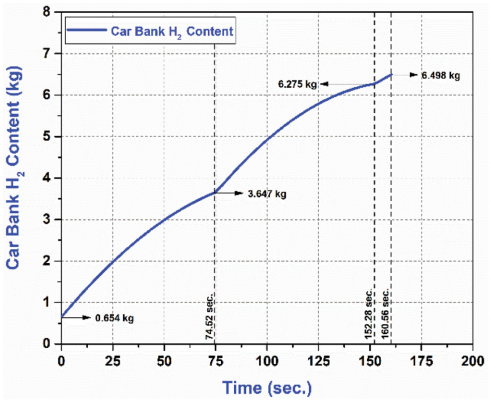


(c) Car tank temperature vs. time.

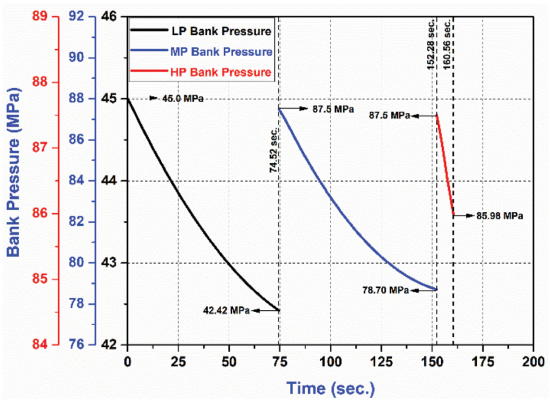


(d) Hydrogen mass flow rate vs. time.

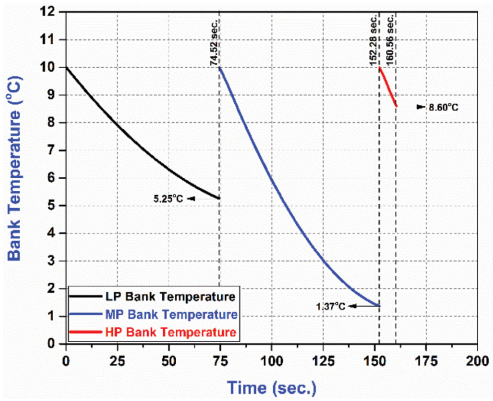
Fig. S3. Case 4 checkpoints results vs. time.



(e) Car tank hydrogen content vs. time.



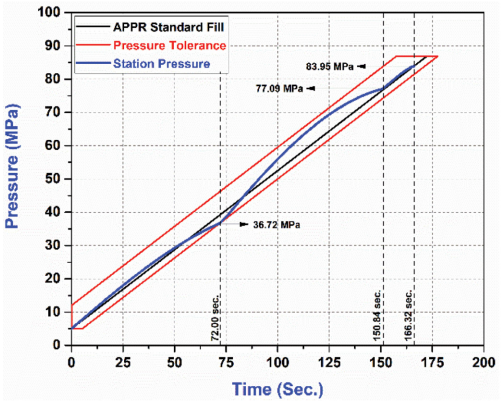
(f) Banks' pressure profile.



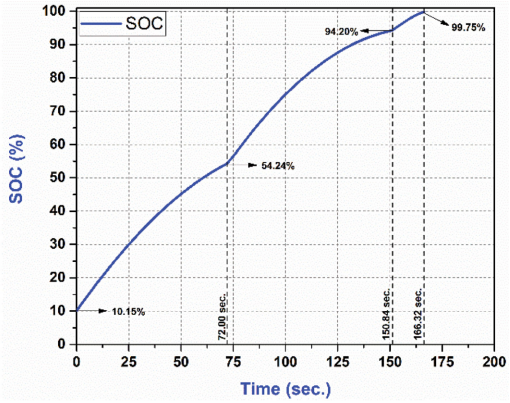
(g) Banks' temperature profile.

Fig. S3. Continued.

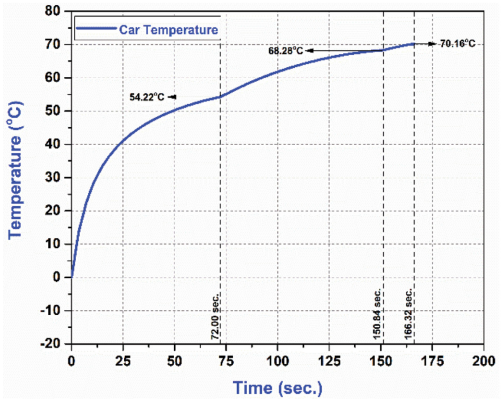
Case 5: 5.0 MPa, 0 °C



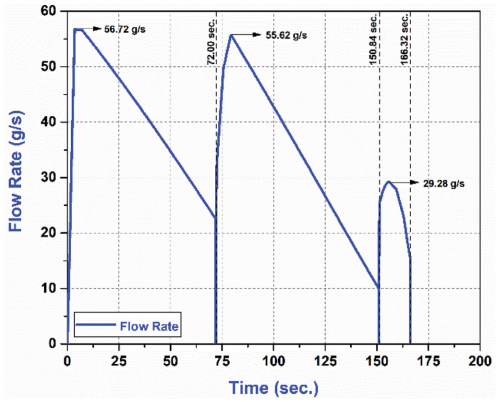
(a) Station pressure vs. time.



(b) State of charge (SOC) % vs. time.

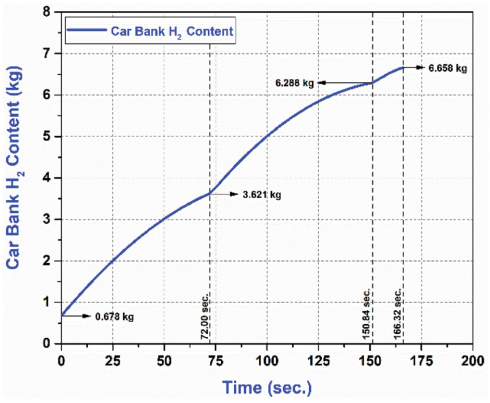


(c) Car tank temperature vs. time.

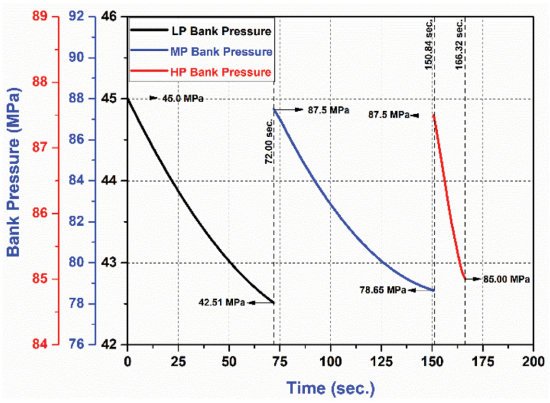


(d) Hydrogen mass flow rate vs. time.

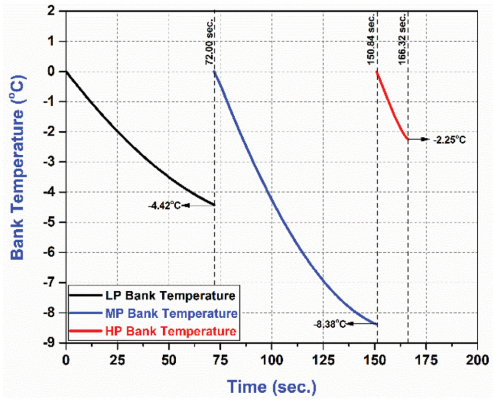
Fig. S4. Case 5 checkpoints results vs. time.



(e) Car tank hydrogen content vs. time.



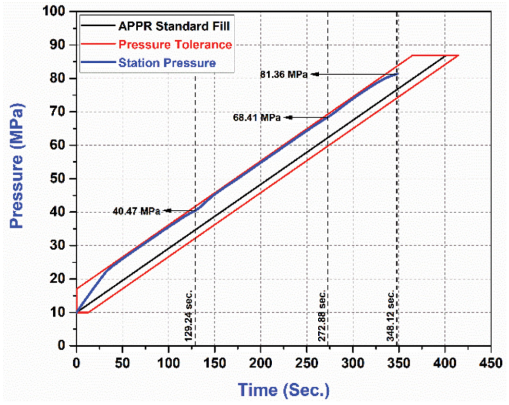
(f) Banks' pressure profile.



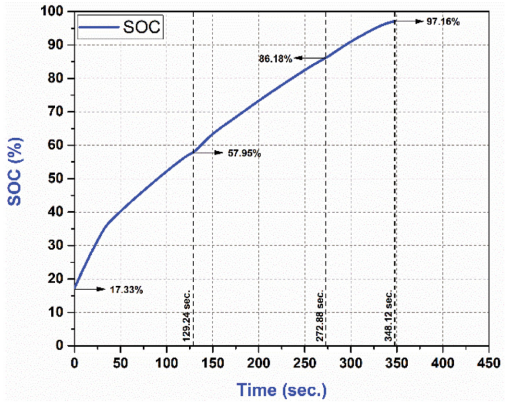
(g) Banks' temperature profile.

Fig. S4. Continued.

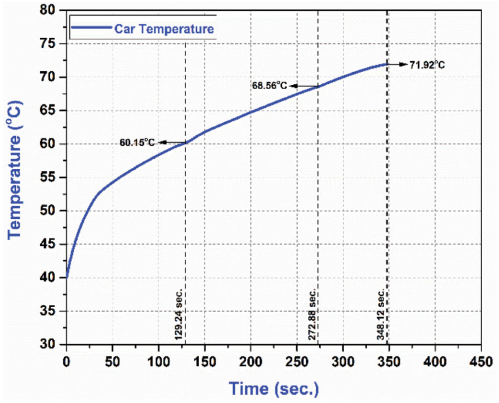
Case 7: 10.0 MPa, 40 °C



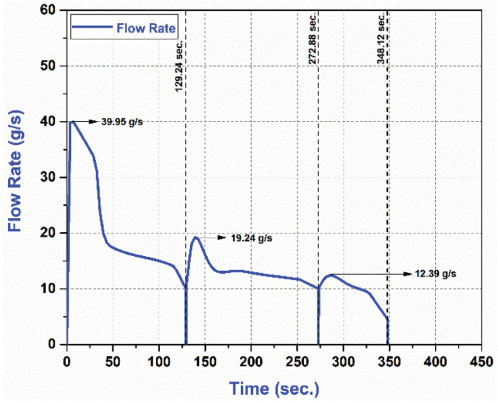
(a) Station pressure vs. time.



(b) State of charge (SOC) % vs. time.

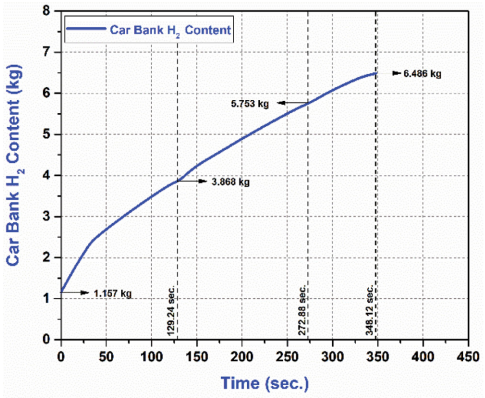


(c) Car tank temperature vs. time.

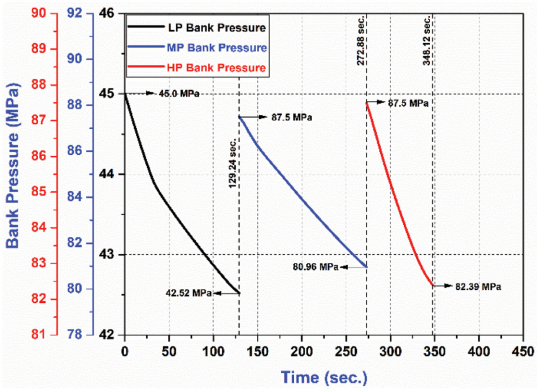


(d) Hydrogen mass flow rate vs. time.

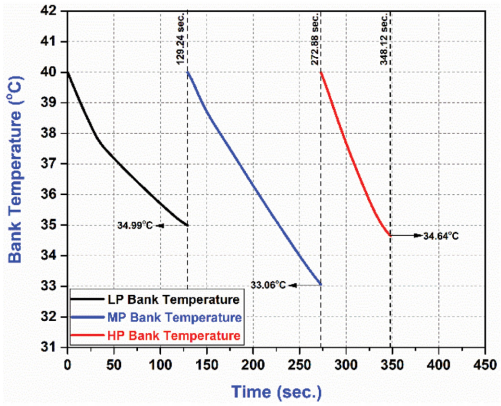
Fig. S5. Case 7 checkpoints results vs. time.



(e) Car tank hydrogen content vs. time.



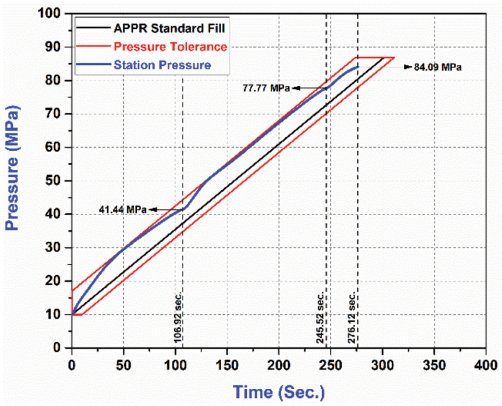
(f) Banks' pressure profile.



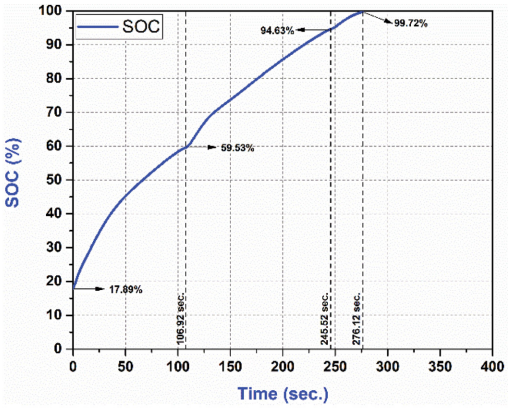
(g) Banks' temperature profile.

Fig. S5. Continued.

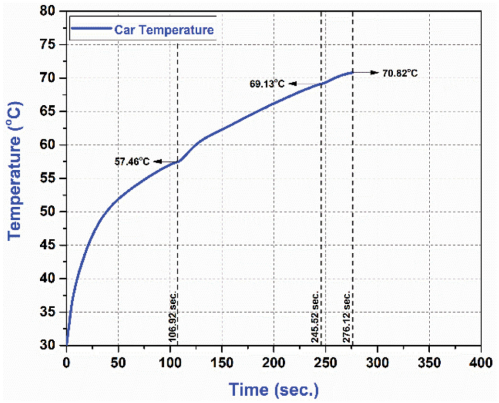
Case 8: 10.0 MPa, 30 °C



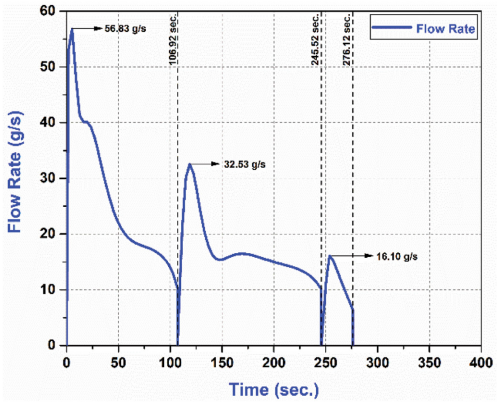
(a) Station pressure vs. time.



(b) State of charge (SOC) % vs. time.

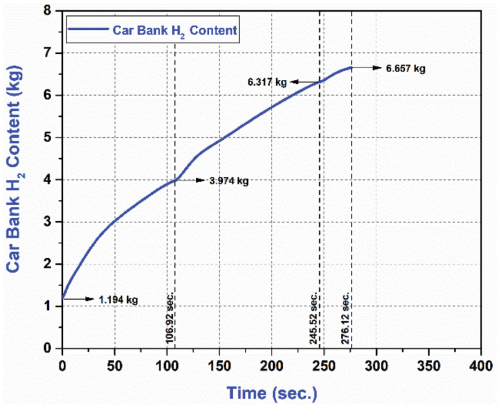


(c) Car tank temperature vs. time.

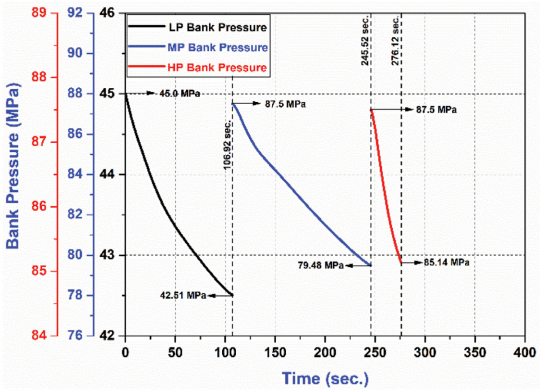


(d) Hydrogen mass flow rate vs. time.

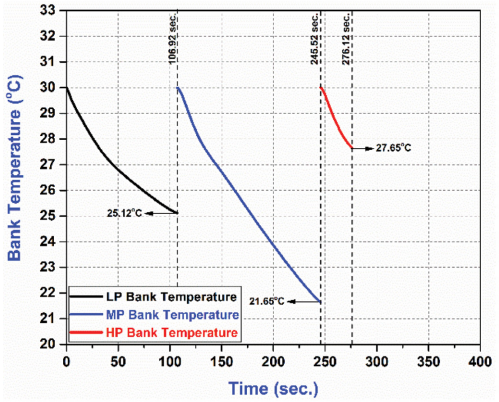
Fig. S6. Case 8 checkpoints results vs. time.



(e) Car tank hydrogen content vs. time.



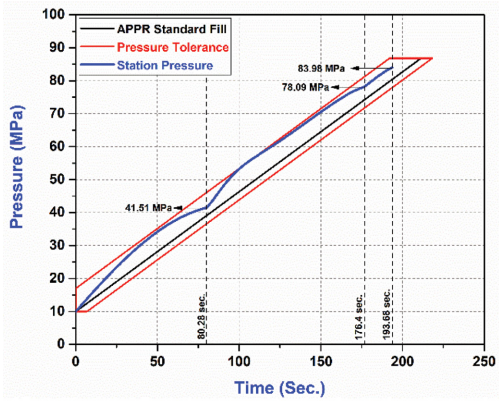
(f) Banks' pressure profile.



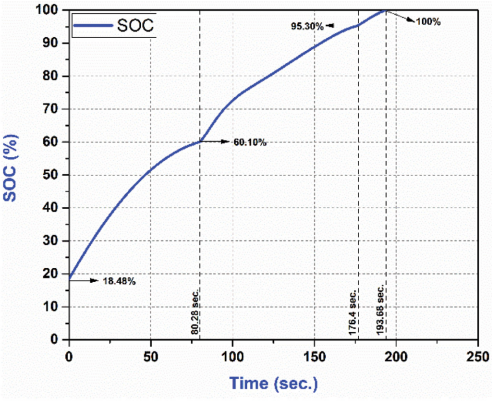
(g) Banks' temperature profile.

Fig. S6. Continued.

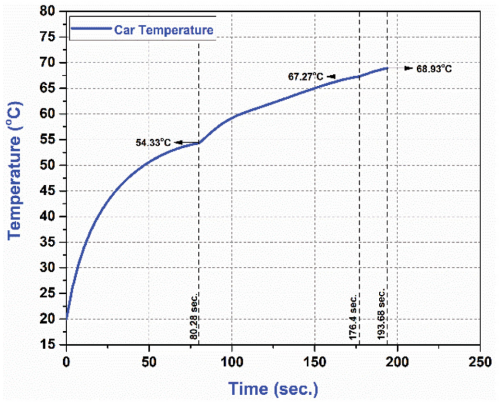
Case 9: 10.0 MPa, 20 °C



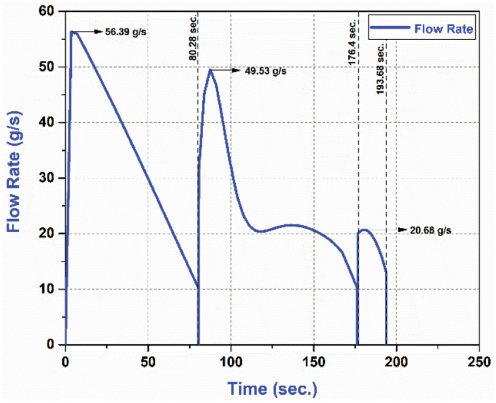
(a) Station pressure vs. time.



(b) State of charge (SOC) % vs. time.

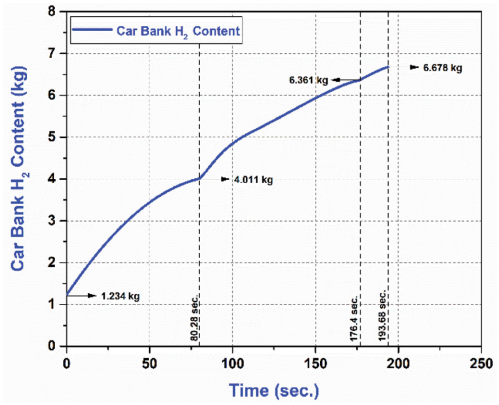


(c) Car tank temperature vs. time.

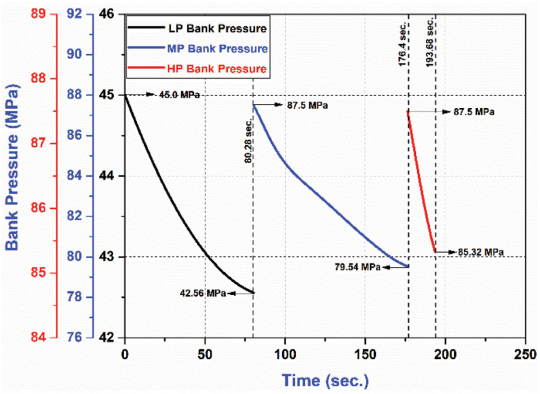


(d) Hydrogen mass flow rate vs. time.

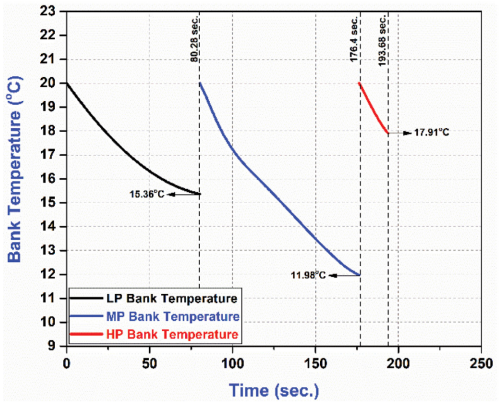
Fig. S7. Case 9 checkpoints results vs. time.



(e) Car tank hydrogen content vs. time.



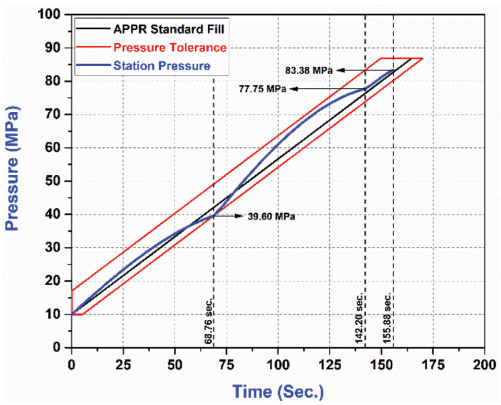
(f) Banks' pressure profile.



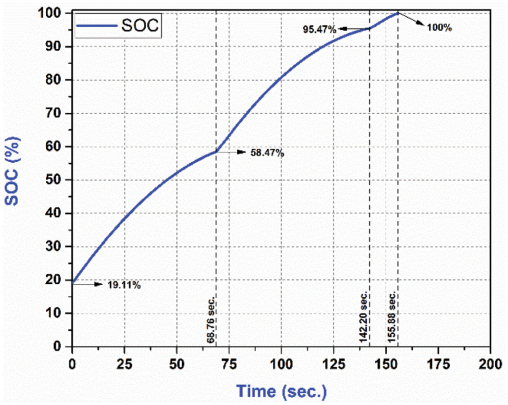
(g) Banks' temperature profile.

Fig. S7. Continued.

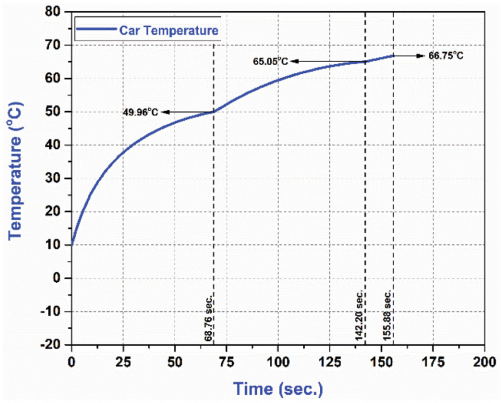
Case 10: 10.0 MPa, 10 °C



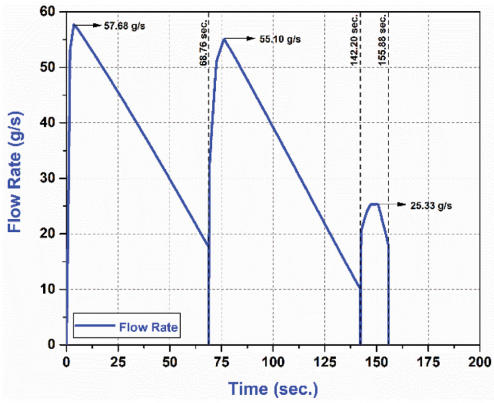
(a) Station pressure vs. time.



(b) State of charge (SOC) % vs. time.

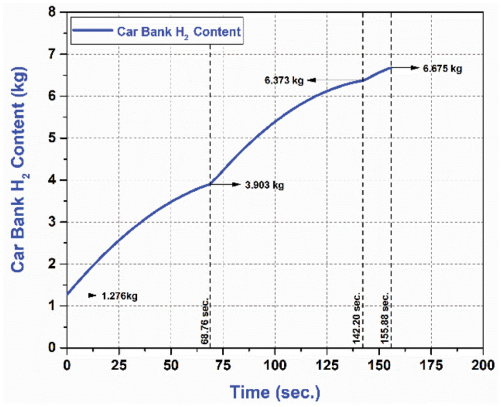


(c) Car tank temperature vs. time.

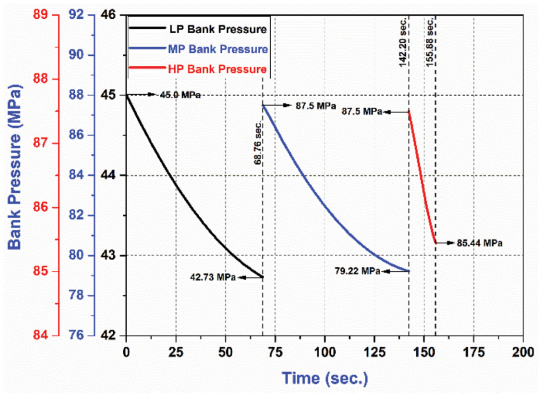


(d) Hydrogen mass flow rate vs. time.

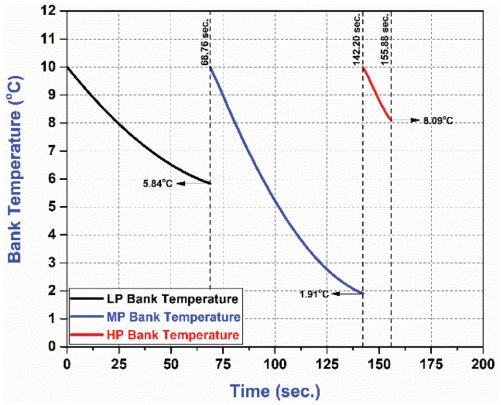
Fig. S8. Case 10 checkpoints results vs. time.



(e) Car tank hydrogen content vs. time.



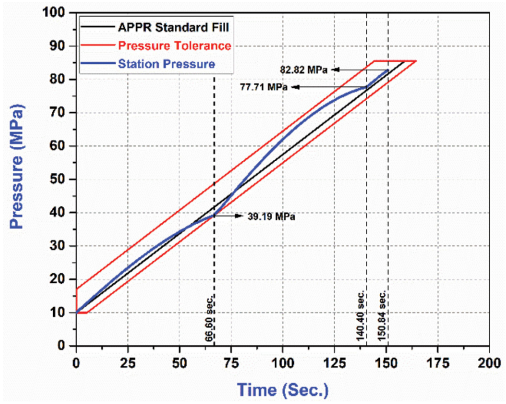
(f) Banks' pressure profile.



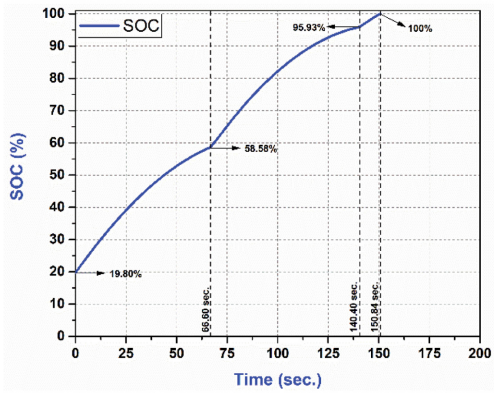
(g) Banks' temperature profile.

Fig. S8. Continued.

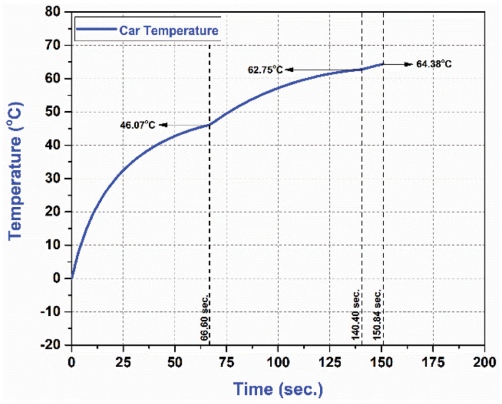
Case 11: 10.0 MPa, 0 °C



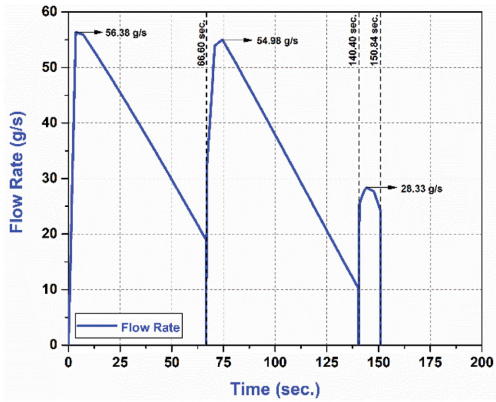
(a) Station pressure vs. time.



(b) State of charge (SOC) % vs. time.

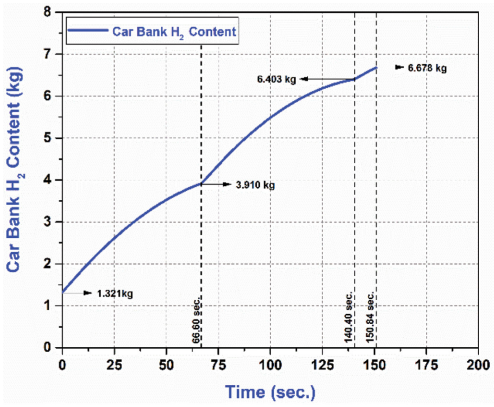


(c) Car tank temperature vs. time.

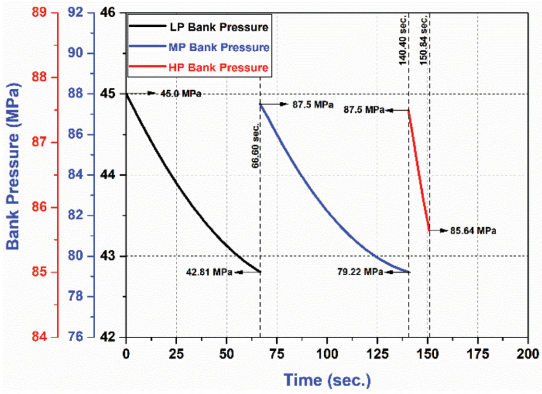


(d) Hydrogen mass flow rate vs. time.

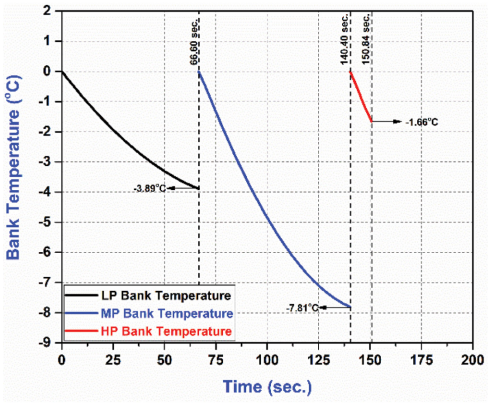
Fig. S9. Case 11 checkpoints results vs. time.



(e) Car tank hydrogen content vs. time.



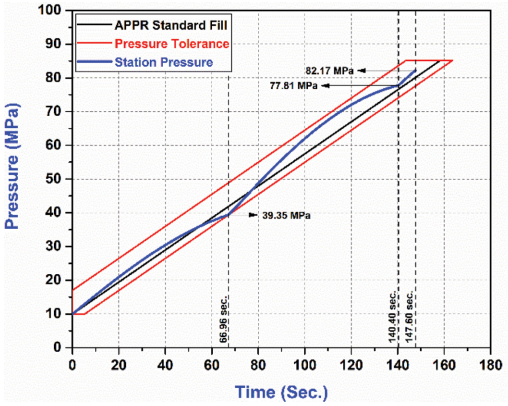
(f) Banks' pressure profile.



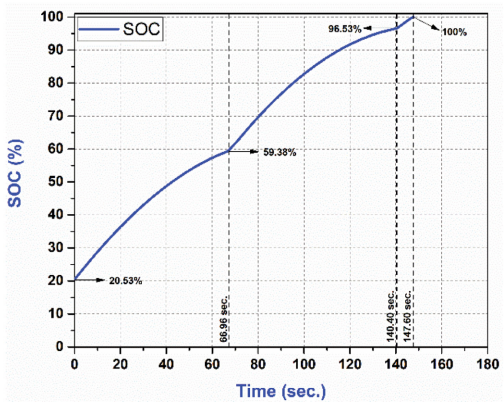
(g) Banks' temperature profile.

Fig. S9. Continued.

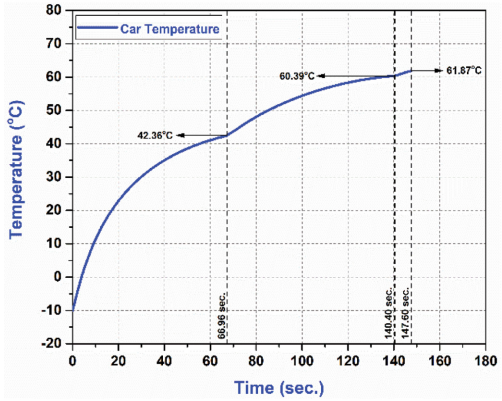
Case 12: 10.0 MPa, −10 °C



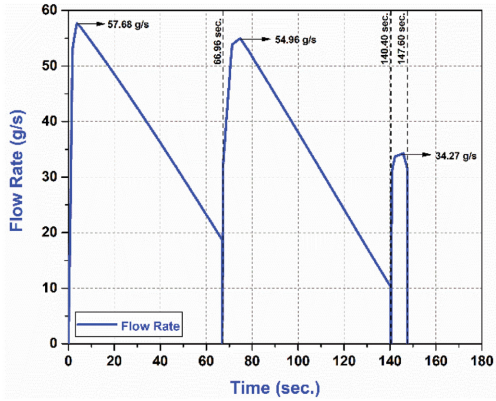
(a) Station pressure vs. time.



(b) State of charge (SOC) % vs. time.

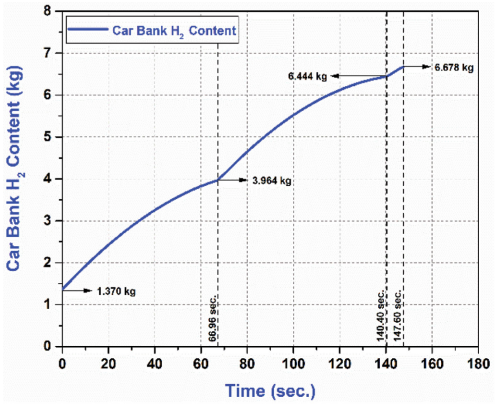


(c) Car tank temperature vs. time.

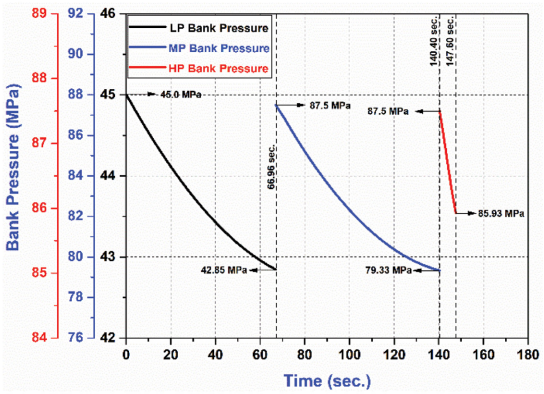


(d) Hydrogen mass flow rate vs. time.

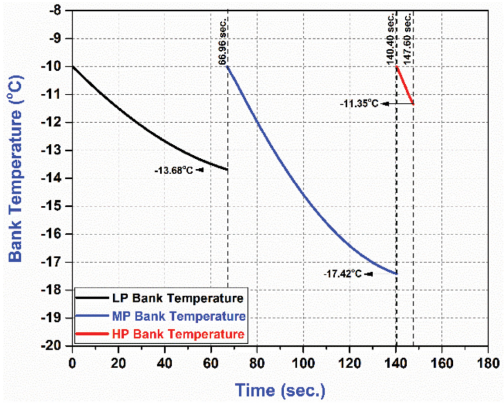
Fig. S10. Case 12 checkpoints results vs. time.



(e) Car tank hydrogen content vs. time.



(f) Banks' pressure profile.



(g) Banks' temperature profile.

Fig. S10. Continued.